Accepted Manuscript

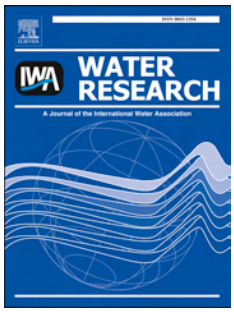

Plant-wide model-based analysis of iron dosage strategies for chemical phosphorus removal in wastewater treatment systems

C. Kazadi Mbamba, E. Lindblom, X. Flores-Alsina, S. Tait, S. Anderson, R. Saagi, D.J. Batstone, K.V. Gernaey, U. Jeppsson

PII: S0043-1354(19)30104-6

DOI: https://doi.org/10.1016/j.watres.2019.01.048

Reference: WR 14416

To appear in: *Water Research*

Received Date: 8 November 2018

Revised Date: 16 January 2019

Accepted Date: 25 January 2019

Please cite this article as: Mbamba, C.K., Lindblom, E., Flores-Alsina, X., Tait, S., Anderson, S., Saagi, R., Batstone, D.J., Gernaey, K.V., Jeppsson, U., Plant-wide model-based analysis of iron dosage strategies for chemical phosphorus removal in wastewater treatment systems, *Water Research*, https://doi.org/10.1016/j.watres.2019.01.048.

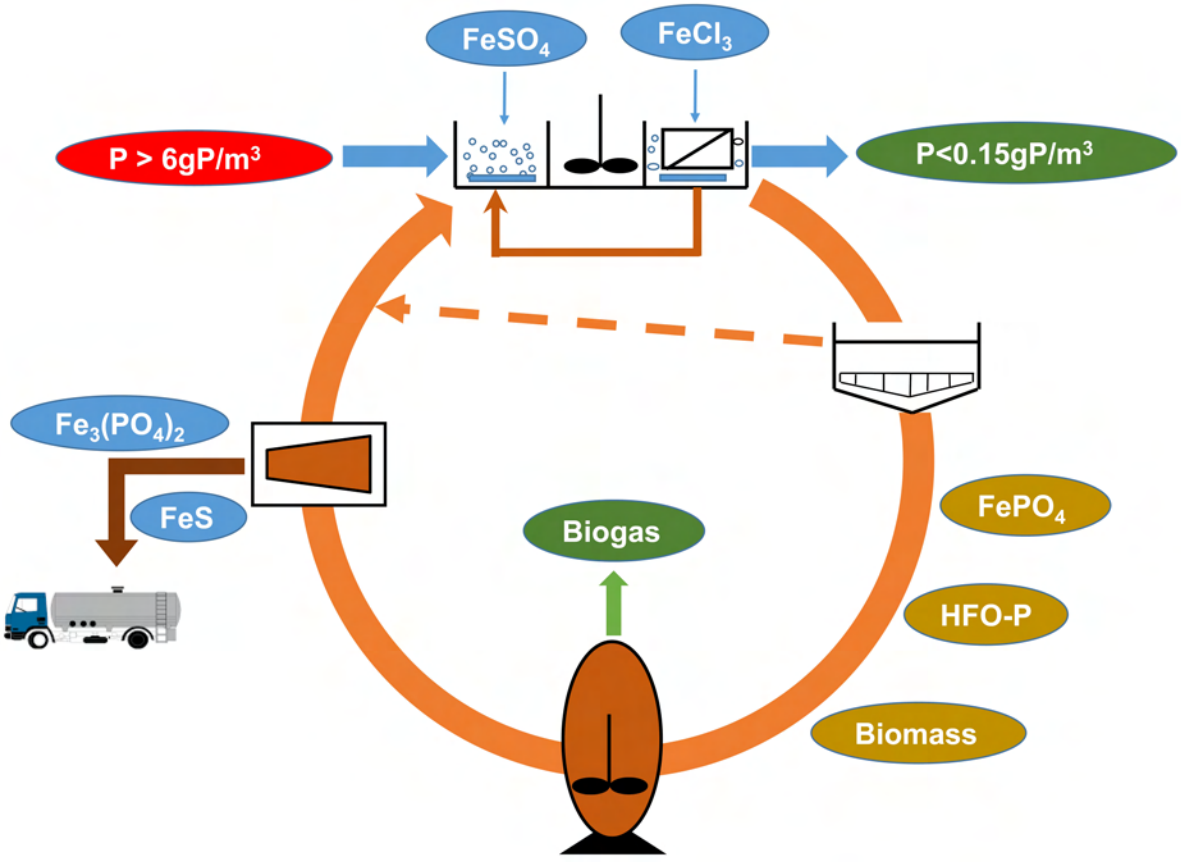

Plant-wide model-based analysis of iron dosage strategies for chemical phosphorus removal in wastewater treatment systems

C. Kazadi Mbamba[1,2], E. Lindblom[2,3], X. Flores-Alsina[4], S. Tait[5], S. Anderson[3], R. Saagi[2], D.J. Batstone[6], K. V. Gernaey[4], U. Jeppsson[2]

[1] RISE Research Institutes of Sweden, Energy and Circular Economy - Urban Water Management, SE - 223 63 Lund, Sweden

[2] Division of Industrial Electrical Engineering and Automation, Department of Biomedical Engineering, Lund University, Box 118, SE-221 00, Lund, Sweden

[3] Stockholm Vatten och Avfall, SE-106 36 Stockholm, Sweden

[4] Process and Systems Engineering Center (PROSYS), Department of Chemical and Biochemical Engineering, Technical University of Denmark, Building 229, DK-2800, Kgs. Lyngby, Denmark

[5] Centre for Agricultural Engineering, University of Southern Queensland, Toowoomba, Queensland, 4350, Australia

[6] Advanced Water Management Centre, The University of Queensland, St Lucia, Brisbane, Queensland, 4072, Australia

Corresponding author:

Christian Kazadi Mbamba

christian.kazadi.mbamba@ri.se

Abstract

Stringent phosphorus discharge standards (i.e. 0.15 – 0.3 g $P.m^{-3}$) in the Baltic area will compel wastewater treatment practice to augment enhanced biological phosphorus removal (EBPR) with chemical precipitation using metal salts. This study examines control of iron

chemical dosing for phosphorus removal under dynamic loading conditions to optimize operational aspects of a membrane biological reactor (MBR) pilot plant. An upgraded version of the Benchmark Simulation Model No. 2 (BSM2) with an improved physico-chemical framework (PCF) is used to develop a plant-wide model for the pilot plant. The PCF consists of an equilibrium approach describing ion speciation and pairing, kinetic minerals precipitation (such as hydrous ferric oxides (HFO) and $FePO_4$) as well as adsorption and co-precipitation. Model performance is assessed against data sets from the pilot plant, evaluating the capability to describe water and sludge lines across the treatment process under steady-state operation. Simulated phosphorus differed as little as 5–10% (relative) from measured phosphorus, indicating that the model was representative of reality. The study also shows that environmental factors such as pH, as well operating conditions such as Fe/P molar ratios (1, 1.5 and 2), influence the concentration of dissolved phosphate in the effluent. The time constant of simultaneous precipitation in the calibrated model, due to a step change decrease/increase in $FeSO_4$ dosage, was found to be roughly 5 days, indicating a slow dynamic response due to a multi-step process involving dissolution, oxidation, precipitation, aging, adsorption and co-precipitation. The persistence effect of accumulated iron-precipitates (HFO particulates) in the activated sludge seemed important for phosphorus removal, and therefore solids retention time plays a crucial role according to the model. The aerobic tank was deemed to be the most suitable dosing location for $FeSO_4$ addition, due to high dissolved oxygen levels and good mixing conditions. Finally, dynamic model-based analyses show the benefits of using automatic control when dosing chemicals.

Key words: Iron, Membrane bioreactors, Phosphorus removal, chemical precipitation, Plant-wide model, Wastewater treatment

Nomenclature

ADM1	Anaerobic Digestion Model No. 1	
Al^{3+}	Aluminium ion	
ASM	Activated sludge model	
ASM2d	Activated Sludge Model No. 2d	
BOD_7	7-day biochemical oxygen demand	($gCOD.m^{-3}$)
BR1/ANOX	Anoxic bioreactor 1	
BR2/ANOX	Anoxic bioreactor 2	
BR3/FLEX	Swing bioreactor 3 (anoxic/aerobic)	
BR4/AERO	Aerobic bioreactor 4	
BR5/AERO	Aerobic bioreactor 5	
BR6/DEOX	De-aeration bioreactor 6	
BR7/ANOX	Post-anoxic bioreactor 7	
BSM2	Benchmark Simulation Model No. 2	
Ca	Calcium	($mole.L^{-1}$)
CAS	Conventional activated sludge	
Cl	Chloride	($mole.L^{-1}$)
CO_2	Carbon dioxide	
COD	Chemical oxygen demand	($gCOD.m^{-3}$)
DO	Dissolved oxygen	($g.m^{-3}$)
EBPR	Enhanced biological phosphorus removal	
EPA	Environmental Protection Agency	
Fe	Iron	
$FeCl_3$	Iron chloride	

$FeSO_4$	Iron(II) sulphate	
Iron(II) or Fe^{2+}	Ferrous iron	(mole.L^{-1})
Iron(III) or Fe^{3+}	Ferric iron	(mole.L^{-1})
ISS	Inorganic suspended solids	(gSS.m^{-3})
K	Potassium	(mole.L^{-1})
MBR	Membrane bioreactor	
Mg	Magnesium	
MLSS	Mixed liquor suspended solids	(gSS.m^{-3})
n	Order of the precipitation reaction	
Na	Sodium	
NH_3	Ammonia	
NH_4-*N*	Ammoniacal nitrogen	(gN.m^{-3})
NO_3-*N*	Nitrate nitrogen	(gN.m^{-3})
O_2	Oxygen	
pH	Hydrogen potential	(standard)
PO_4^{3-}	Phosphate ion	
PO_4-*P*	Orthophosphate phosphorus	(gP.m^{-3})
RAS	Returned activated sludge	
S_A	Fermentation products	(gCOD.m^{-3})
S_F	Readily biodegradable organics	(gCOD.m^{-3})
S_I	Inert biodegradable organics	(gCOD.m^{-3})
S_{O2}	Dissolved oxygen	(g.m^{-3})
t	Time	(min, h, day)

T	Temperature	(^{o}C, K)
TIC	Total inorganic carbon	(gC.m^{-3})
TN	Total nitrogen	(gN.m^{-3})
TOC	Total organic carbon	(gC.m^{-3})
TP	Total phosphorus	(gP.m^{-3})
TSS	Total suspended solids	(gSS.m^{-3})
VFA	Volatile fatty acids	(gCOD.m^{-3})
VSS	Volatile suspended solids	(gSS.m^{-3})
WAS	Waste activated sludge	
WWTP	Wastewater treatment pant	
X_{AUT}	Autotrophic biomass	(gCOD.m^{-3})
X_{FePO4}	Iron phosphate mineral state	(gFe.m^{-3})
X_{H}	Heterotrophic biomass	(gCOD.m^{-3})
X_{HFO}	Hydrous ferric oxide	(g.m^{-3})
$X_{HFO,H}$	Hydrous ferric oxide with high adsorption capacity	(g.m^{-3})
$X_{HFO,H,P}$	$X_{HFO,H}$ with adsorbed phosphate	(g.m^{-3})
$X_{HFO,L}$	Hydrous ferric oxide with low adsorption capacity	(g.m^{-3})
$X_{HFO,L,P}$	$X_{HFO,L}$ with adsorbed phosphate	(g.m^{-3})
X_{I}	Inert non-biodegradable organics	(gCOD.m^{-3})
X_{ISS}	Inorganic suspended solids state	(gSS.m^{-3})
X_{PAO}	Phosphorus-accumulating organisms state	(gCOD.m^{-3})
X_{PHA}	Polyhydroxy-alkanoate state	(gCOD.m^{-3})
X_{PP}	Polyphosphate state	(g.m^{-3})

X_S	Slowly biodegradable substrate state	($gCOD.m^{-3}$)
X_{TSS}	Total suspended solids state	($gTSS.m^{-3}$)

49

Research highlights

- A plant-wide model calibrated against extensive pilot-plant data describing phosphorus (P) dynamics with iron (Fe) dosing.
- Good agreement between measured and modelled P (5–10% (relative) difference).
- P concentration strongly depends on pH, Fe/P ratio and influent P load.
- P removal control strategies substantially reduce $FeSO_4$ dose.
- Model shows aerobic tanks are the most suitable dosing location for $FeSO_4$, due to fast oxidation of Fe^{2+} to Fe^{3+}.

1 Introduction

In recent years, effluent discharge limits to receiving waters are becoming more stringent, owing to increased awareness and growing concerns regarding pollution and degradation of water resources. For example, current effluent standards in Stockholm (Sweden) restrict the concentrations of total phosphorus (TP) in treated wastewater discharge to less than 0.3 $gP.m^{-3}$. However, these requirements are expected to be tightened to achieve more efficient phosphorus removal. The future annual average emission standards for TP in Stockholm, Sweden, will likely be 0.2 $gP.m^{-3}$, with the operational effluent target set at 0.15 $gP.m^{-3}$ (Anderson *et al.*, 2016). To meet these stricter quality standards, the effluent should contain very low concentrations of dissolved phosphorus and almost no suspended solids. Wastewater treatment facilities will need to undergo significant (structural/operational) modifications and/or improvements as far as nutrient removal is concerned. A number of existing wastewater treatment plants are seeking to intensify treatment using conventional activated sludge (CAS) systems coupled with membrane solids separation referred to as membrane bioreactors (MBRs) (Judd, 2008). Since MBR systems have high selectivity and can be operated with high suspended solids concentrations and longer sludge retention times, a smaller footprint results. Consequently, biological nutrient removal in MBRs is becoming more

74 popular as a means of treating wastewater and has now been successfully achieved at lab-, pilot and full-
75 scale (Bertanza *et al.*, 2017; Wang *et al.*, 2014).

76 In terms of biological treatment options, enhanced biological phosphorus removal (EBPR) is now
77 common practice. However, the feasibility of EBPR systems may be limited to some extent (Ekama,
78 2010) by wastewater characteristics and other environmental factors such as temperature and mass
79 loading. In such situations, phosphorus (P) removal by biological means can be supported by chemical
80 precipitation processes (De Haas *et al.*, 2000a). In current practice, chemical phosphorus removal in
81 conventional activated sludge plants is mainly performed by the addition of iron (Fe) or aluminium salts
82 upstream of the primary clarifier (pre-precipitation), to mixed liquor in the activated sludge tanks
83 (simultaneous precipitation or co-precipitation) and/or to the tertiary processes (post-precipitation)
84 (Henze *et al.*, 2002; EPA, 2010). The phosphorus removal efficiency depends on a number of factors
85 including pH, temperature, redox conditions, dosing location, reactor configuration, and iron and
86 phosphorus conversions by microorganisms present in the wastewater (De Haas *et al.*, 2000a; Wang *et*
87 *al.*, 2014). In turn, these factors will dictate the forms of iron, either ferric (Fe^{3+}) or ferrous (Fe^{2+}), and
88 influence the rate and extent of iron transformations. As an illustration, when ferric salts are added to the
89 mixed liquor, the salt ionizes to yield the free metallic ions, a portion of which may then react with
90 orthophosphate (PO_4-P) to form insoluble ferric phosphate precipitates (strengite). The precipitates might
91 then be separated out by sedimentation or membrane filtration (Wu *et al.*, 2015). However, the majority
92 of ferric ions will combine with hydroxide ions to form a variety of hydroxide complexes, termed hydrous
93 ferric oxides (HFO) with high sorption capacity, which will subsequently assist in the removal of
94 phosphorus by adsorption and co-precipitation (Smith *et al.*, 2008). Due to high costs of ferric iron salts,
95 Fe is in some instances added as ferrous iron, such as in $FeSO_4$ salt, which may oxidize to Fe^{3+} at the
96 dosing point if oxidizing conditions prevail in the physical or biological treatment stage (EPA, 2010). In
97 order to achieve greater degrees of P removal, higher levels of iron or smarter dosing strategies may be
98 required (e.g. optimum dosing location, molar ratio requirements).

For MBR systems, and for CAS plants without tertiary treatment, biological treatment is usually the final treatment step, which means that the process will have to operate with much lower phosphorus concentrations. Phosphorus is an essential nutrient for microbial growth and its shortage may limit biological activities, such as nitrification and denitrification processes (Philips *et al.*, 2003). This introduces a sensitive interaction between biology and precipitation chemistry, requiring optimal phosphorus removal control strategies and operational settings to achieve efficient and robust wastewater treatment. A more detailed insight into the interactions between iron species and phosphorus within a biological nutrient system with membrane separation is of particular importance to many countries. Wastewater utilities are assessing biological nutrient removal with MBRs to establish a suitable treatment pathway in line with stricter discharge requirements in the future (Daigger *et al.*, 2010). While current studies have significantly increased knowledge of the process design with membrane technology and modified biological treatment, there is still a need to further clarify the impacts of ferric and ferrous iron dosing on phosphorus removal in the activated sludge system. Gaining insight into iron speciation and iron species transformation through modelling is paramount to capture the mechanisms of iron-precipitation, as their nature, movement and fate in bioreactors would impact both phosphorus removal efficiency as well as membrane performance characteristics.

A recent study proposed a mechanistic chemical P removal modelling approach, which describes the kinetics precipitation and flocculation of HFO as well as P adsorption onto HFO particulates and co-precipitation (Hauduc *et al.*, 2015). This model had been calibrated and validated with lab-scale data on P removal with iron in synthetic aqueous solutions. The model framework of Hauduc *et al.*, (2015) was demonstrated to be well-suited for benchmark development procedures for optimizing control and operational strategies for chemical dosing in a plant-wide context (Solon *et al.*, 2017), however this approach has not been validated with real wastewater for full-scale implementation. By the way of contrast, Kazadi Mbamba *et al.* (2016) validated a phosphorus plant-wide model with spontaneous precipitation in anaerobic digestion, but did not include simultaneous precipitation of P with metals in the

activated sludge system. The main reason of excluding simultaneous precipitation by Kazadi Mbamba *et al.* (2016) was that P was solely removed by biological processes in the modelled full-scale system. Consequently, the approach of Hauduc *et al*. (2015) and the plant-wide model of Solon *et al*. (2017) have not yet been tested on full-scale data with diverse dynamics, and this is the focus of the present study.

The main novelty of this contribution is to predict P and Fe transformations in both water and sludge lines. Current modelling approaches and understanding of the reaction mechanisms of iron and phosphorus are applied to pilot-scale data to evaluate control and operational strategies. The study also focuses on the impact of the Fe/P molar ratio system when the pH varies, and its effect on effluent TP concentration, for example due to routine membrane cleaning with acidic solutions. Special focus is placed on validating these aspects using recent model development. The paper is structured to first present the underlying principles of the plant-wide model including the precipitation model, then the validation step with static pilot-test data and other steady-state analyses, after which dynamic simulations are used to examine the influence of operational and control factors.

2 Methodology

2.1 Pilot-plant configuration

The MBR pilot-plant under study is located at the R&D facility Hammarby Sjöstadsverk, which is adjacent to Henriksdal wastewater treatment plant (WWTP) (850,000 PE), the largest in Stockholm (Sweden). The purpose of the pilot-plant is to evaluate the design of a future full-scale facility and optimize operation and control. The pilot-plant design mimics the configuration of the future full-scale facility, which consists of pre-aeration tanks, primary clarifiers and membrane bioreactors with anoxic and aerated zones. The scale factor used in the design and rebuilding of the pilot-plant compared with the

full-scale plant is 1:6,700, except for the primary sedimentation, which is relatively small (scale factor 1:12,000), and as a result led to poorer Total Suspended Solids (TSS) separation efficiency than would be expected from full-scale. A major difference for the operating strategy and control between pilot and full-scale, is that the pilot has only two membrane tanks that can be put into operation for optimal/energy efficient membrane operation, whereas each line in the full-scale system will have 12 membrane tanks.

The pilot-plant treatment process consists of a conventional primary treatment including a pre-aeration step, where $FeSO_4$ is added, followed by seven bioreactors operated as a 4-stage modified Ludzack-Ettinger (MLE) process consisting of two anoxic (BR1/ANOX and BR2/ANOX), one aerobic/anoxic (BR3/FLEX), two aerobic (BR4/AERO and BR5/AERO), one de-oxygenation (BR6/DEOX) and one post-anoxic (BR7/ANOX) compartments (Figure S1 and Table S1). The Henriksdal wastewater treatment plant consists of two influents: Sickla influent (SIN) and Henriksdal influent (HIN). The influent to the pilot-plant was derived from HIN.

From the mixed liquor suspended solids (MLSS) in the membrane bioreactor tanks, clarified permeate for final discharge is produced. The retentate from the MBRs is distributed to the bioreactors as returned activated sludge (RAS), while a small portion is bled as waste activated sludge (WAS). A sludge treatment facility was constructed at the pilot-plant but not yet in operation during this project; however, anaerobically digested supernatant (Table 1) from Henriksdal WWTP was blended with the RAS flow in the RAS-deoxygenation zone (RASDEOX) and then fed to the first anoxic reactor.

Although the pilot-plant during the time of the study did not have an operational sludge treatment train (anaerobic digester), an interaction with sludge treatment was physically simulated by adding digestate back into the membrane module and routinely removing WAS and primary sludge from the pilot-plant.

2.2 Membrane bioreactors

The MBR pilot uses GE hollow fiber membranes (nominal pore size 0.04 μm) with two cassettes (2.5m x 1.0m x 0.34m) of three membrane modules each, immersed in each membrane tank. Each module has a membrane area of 34.2 m^2 and consists of a variety of fiber strands with attachment at the top and bottom of the cassette frame. The filtered water (permeate) is transported on the inside of the fibers to connections in both the bottom and the top of the module. The membranes are kept clean during operation by aeration from below and backpulse cleaning-in-place (CIP) with hypochlorite and citric/oxalic acid solution twice per week, respectively. The bioreactors are operated with a hydraulic retention time (HRT) of 12 hours and a sludge retention time (SRT) of about 23 days. The membrane modules are operated in cyclic mode with 9 minutes of filtration at a constant flux of 19.4 $L.m^{-2}.h^{-1}$ (LMH) followed by a 1 minute relaxation.

2.3 Chemical addition

Phosphorus was removed from the aqueous phase by chemical precipitation, dosing $FeSO_4 \cdot 7H_2O$ (iron (II) sulfate heptahydrate) and $FeCl_3 \cdot 6H_2O$ (iron (III) chloride hexahydrate) at three distinct dosing points. $FeSO_4$ was dosed in the pre-aeration tank before the primary clarifier and in the aerobic tank (BR4/AEROB), whereas $FeCl_3$ was added at the end of the post-denitrification (BR7/ANOX) before the membrane tanks. The addition of $FeSO_4$ to the pre-aeration tank was flow-proportional with an annual average dose of 10 $gFe.m^{-3}$, while the addition of $FeSO_4$ in the BRA4/AEROB was controlled to achieve a set point of 0.2 $gP.m^{-3}$ in the treated effluent, with a maximum dose of 15 $gFe.m^{-3}$. $FeCl_3$ added before the membrane tanks was also controlled to achieve a set point of 0.15 $gP.m^{-3}$ in the effluent, with a maximum dose of 15 $gFe.m^{-3}$. Brenntaplus (a mixture of proteins, sugars and alcohols) with concentration of about 400,000 $gCOD.m^{-3}$ was used as an external carbon source. It was dosed at a flowrate of 0.005 $m^3.d^{-1}$ in the post-anoxic tank (BR7/ANOX) and the dosage was controlled to achieve a pre-selected nitrate concentration set point of 3 $gN.m^{-3}$ in the effluent.

2.4 Influent characterisation

2.4.1 Routine measurement data

A SCADA (supervisory control and data acquisition) system provided the following daily data: (1) flow rates of water and sludge streams, (2) air flow rate to the activated sludge system, (3) phosphate phosphorus (PO_4-P), (4) nitrate nitrogen (NO_3-N) in treated effluent, (5) dissolved oxygen (DO), (6) total suspended solids (SS), (6) temperature and (7) pH in membrane tank 2. In addition, the operating utility (Stockholm Vatten och Avfall (SVOA)) provided data from routine sampling and off-line analysis which included daily and weekly measurements on composite samples from auto-samplers located at the influent, primary effluent, effluent, bioreactor 4 and RASDEOX line. Analyses on the influent and effluent included total organic carbon (TOC), 7-day biological oxygen demand (BOD_7), TSS, volatile suspended solids (VSS), total dissolved solids (TDS), volatile fatty acids (VFA), ammoniacal nitrogen (NH_4-N), NO_3-N, total nitrogen (TN), PO_4-P, total phosphorus (TP), alkalinity, iron (Fe) soluble calcium (Ca), magnesium (Mg), sodium (Na) and potassium (K). Analyses were generally done using Standard Methods (APHA, 2012). The samples were conserved with 1-part 4M sulfuric acid to 100 parts sample volume, except for samples tested for TOC, which were instead conserved with 2M hydrochloric acid in the same proportions. In addition to external analyses, other samples, as described in Section 2.4.2, were analysed internally (on site) for TSS, filtered and total COD, TN and NH_4-N by colorimetric methods using a spectrophotometer (WTW Photolab 6600). Data collected over a period from 20 June 2016 to 10 April 2017 were selected and averaged, before use as a representative measure of steady state conditions.

2.4.2 Additional data measuring campaign

Additional sampling and off-line analyses were required for model calibration, these were carried out to augment routine measurements at the pilot-plant. Grab and composite samples were collected daily for a week during the period 12/07/2017 to 19/07/2017, from five different points: influent, primary effluent, effluent, from one of the bioreactors (BR4/AEROB) and RASDEOX return sludge. Samples were stored

in a cooler box with ice bricks and transported to an external laboratory (Eurofins Environment Sweden AB), which conducted the analyses.

2.5 New model configuration describing plant wide P-Fe interactions

2.5.1 Plant wide model

The plant-wide model was adapted from the Benchmark Simulation Model No. 2 (BSM2) (Gernaey *et al.*, 2014, Solon *et al.*, 2017). The primary clarifier was modelled as one non-reactive settler (Otterpohl and Freund, 1992). Biokinetics in the activated sludge plant were described by ASM2d (Henze *et al.*, 2000), expanded to include physico-chemical processes as described below in Section 2.5.2. Furthermore, the TSS in ASM2d was computed from volatile suspended solids (VSS) and inorganic suspended solids (ISS) (Ekama and Wentzel, 2004). The membranes were simply described as a reactive filtration system with wastewater entering at the bottom, permeate exiting at the top of the membranes and retained biomass leaving from the base to be recycled back to the activated sludge system as RAS. Sludge thickening and dewatering units were assumed to be ideal (with constant split fraction and characteristics) with no hold-up volume or reactions (Jeppsson *et al.*, 2007).

The pilot-plant during the time of the study did not have a sludge treatment train, but had WAS removed and digestate added to simulate the physical interaction between the liquid and sludge lines (See Section 2.1). To capture this interaction in the model, an anaerobic digester was included on the thickened sludge line (Figure 2). This allowed a full evaluation on the impacts of iron salts to be carried out in the pilot-plant as a whole. Biochemical conversion processes in the anaerobic digester were described by the ADM1 (Batstone *et al.*, 2002), upgraded to include recent developments, including physico-chemical and biological iron, sulphur and phosphorus transformations (Flores-Alsina *et al.*, 2016). For a full exposition of the extended ADM1 model, as well as a detailed description on the matrix format used to represent the anaerobic digestion model, the original publications (Batstone *et al.*, 2002; Solon *et al.*, 2017) can be consulted. Model interfaces were used to translate state variables between the ASM2d and ADM1 and

239 between the ADM1 and the ASM2d, based on continuity principles (Nopens *et al.*, 2009), and in
240 accordance with Solon *et al.* (2017).

241 The membrane model consisted of a simple reactive filter to describe the cycling of RAS between the
242 membrane module and the activated sludge line. Membrane fouling was not considered in the model to
243 minimise unnecessary model complexity, because it would require a large number of parameters to
244 calibrate a fouling model. Also, backwashing and relaxation were not physically modelled. However,
245 aeration for controlling membrane fouling was incorporated in the MBR model to evaluate its impact on
246 the activated sludge treatment.

247 2.5.2 Physico-chemical framework describing Fe precipitation and oxidation/reduction reactions

248 The activated sludge model was extended with the chemical precipitation processes of two minerals,
249 namely hydrous ferric oxide and iron phosphate (strengite, $FePO_4.2H_2O$). Removal of P by chemical
250 precipitation and sorption were assumed to take place in parallel, and were therefore competing for ferric
251 iron in the wastewater within the bioreactors (Wu *et al.*, 2015). Iron transformations were described using
252 the hydrous ferric oxide (HFO) model, which describes how the precipitation of freshly formed and
253 highly reactive HFO provides a number of adsorption sites for ions on its surface (Hauduc *et al.*, 2015).
254 However, a simplified HFO model was used (Solon, 2017; SUMO, 2018). Briefly, the HFO model
255 describes the precipitation of amorphous iron hydroxide or HFO particulates (X_{HFO}), phosphate
256 adsorption/binding onto X_{HFO} and the ageing of HFO as the extent of crystallinity increases. HFO initially
257 precipitates with a high adsorption capacity ($X_{HFO,H}$), which has an open structure and easily accessible
258 binding sites. Through the aging process, X_{HFO} loses reactivity and develops a more compact structure
259 and less accessible sites (thus high reactivity $X_{HFO,H}$ transforms over time into low reactivity $X_{HFO,L}$).
260 Adsorption of phosphates onto HFO leads to production of HFO with bound phosphate ($X_{HFO,H,P}$ or
261 $X_{HFO,L,P}$). The binding of P to $X_{HFO,H,P}$ in the model description is reversible, which means that a

transformation of $X_{HFO,H}$ into $X_{HFO,L}$ in the model would decrease the concentration of $X_{HFO,H}$ and thereby induce a transformation of $X_{HFO,H,P}$ into $X_{HFO,H}$ as well as cause a release of P.

When iron salts, such as $FeSO_4$, are added to the aerobic tank, Fe^{2+} will undergo oxidation into ferric iron as follows:

$$Fe^{2+} + ¼\ O_2 + H^+ \rightarrow Fe^{3+} + ½\ H_2O \quad (3)$$

The reaction consumes a stoichiometric amount of 0.14 g O_2/g Fe^{2+}. The oxidation of ferrous iron leads to the formation of ferric iron and subsequently to HFO precipitates, which will affect the removal of P by adsorption and co-precipitation through the HFO pathway as shown above. The complete stoichiometry and kinetic rates used for the HFO model can be found in Solon (2017).

Direct iron phosphate precipitation (X_{FePO4}) was described as a reversible process using supersaturation as the chemical driving force. The model consisted of two parts; an algebraic equation set for aqueous-phase reactions (weak acid-base and ion-pair equilibrium) and rate expressions for minerals precipitation, minerals dissolution and gas transfer (Kazadi Mbamba *et al.*, 2015a; b).

In the extended ADM1 (Solon *et al.*, 2017), mineral precipitation is also described as a reversible process using supersaturation as the chemical driving force. The multiple minerals in the extended ADM1 include calcite, aragonite, amorphous calcium phosphate and struvite. Furthermore, the extended ADM1 includes iron phase transformation. Ferric iron in the form of hydrous ferric oxides ($X_{HFO,L}$, $X_{HFO,H}$) undergoes reduction to ferrous iron using hydrogen and sulfide as electron donor (Solon *et al.*, 2017). Once released, Fe^{2+} can preferentially bind with S^{2-} to form iron sulphide. Additionally, Fe^{2+} in excess may also combine with soluble phosphate present in the anaerobic digester to form vivianite ($Fe_3(PO_4)_2$). $FePO_4$, if undersaturated, may undergo dissolution releasing Fe^{3+} and soluble P.

Gas transfer in the plant-model was described using single-film mass transfer-controlled processes (Batstone *et al.*, 2002). The gases included were O_2 and CO_2 in ASM2d, and CO_2, NH_3, H_2O and CH_4 were modelled in ADM1.

2.6 Ancillary elements

2.6.1 Influent COD fractions

The fractionation of COD in the influent was performed using the routinely analysed data provided by the pilot-plant operator. As in ASM2d, the COD fractions in the influent included readily biodegradable organic compounds (fermentable) (S_F), fermentation products (S_A), inert soluble organic compounds (S_I), slowly biodegradable organic compounds (X_S) and inert particulate organic compounds (X_I), using a physico-chemical and biological characterization method (Roeleveld *et al.*, 2002). Particulate components, namely heterotrophic organisms (X_H) were considered to be 6% of the influent total COD while the nitrifying organisms (X_{AUT}) were assumed to be negligible in the influent as per Henze *et al.* (1995). Total suspended solids (X_{TSS}), total dissolved ammonia nitrogen (S_{NH4}), nitrate (S_{NO3}) and inorganic soluble phosphorus (S_{PO4}) were assumed to be equal to experimentally measured values, while the remaining variables in the influent, including dissolved oxygen (S_{O2}) and dissolved dinitrogen (S_{N2}), were set to zero.

2.6.2 Synthetic influent data generation

The static influent fractions obtained from the analyses above, were used to determine dynamic influent base characteristics. A simplified dynamic influent generator was used to re-create long-term wastewater dynamics (Gernaey *et al.*, 2011; Flores-Alsina *et al.*, 2014). Since data related to influent wet weather flow-rate conditions were missing for the pilot system, the measured flow rate data were used instead. A temperature module was not included in the model, because measured temperature data were available

and used instead. Finally, an additional module had to be included in the model in order to capture the dynamics of cations (Na, K, Ca, Mg) and anions (Cl) in the influent.

2.6.3 Calibration procedure and more parameters

A step-wise calibration procedure was used (Kazadi Mbamba *et al.,* 2016), whereby kinetic parameters were adjusted to minimize discrepancies between the model outputs and static measured data from the pilot-plant. Besides the influent characterisation described above and adjustment of the maximal rate of autotrophic biomass (0.5 d^{-1}) and decay of autotrophic bacteria (0.1 d^{-1}), model parameters for ASM2d and ADM1 were kept at default values (Henze *et al.*, 2000; Batstone *et al.*, 2002; Flores-Alsina *et al.*, 2016). The Davies approximation to activity coefficients was used with temperature correction, and equilibrium constants were also adjusted for temperature using the constant-enthalpy form of the van't Hoff equation (Stumm & Morgan, 1996). For minerals precipitation reactions in the anaerobic digester, precipitation rate coefficients from a previous study were used (Kazadi Mbamba *et al.*, 2015b).

2.7 Scenario analyses

Scenario analyses were used to investigate the performance of the plant-wide model and the impact of simultaneous precipitation on phosphorus removal under dynamic conditions. The criteria that were used to assess model performance, were related to effluent quality in the water line, including NH_4-N, NO_3-N and PO_4-P. The following six scenarios were assessed:

i) Scenario 1 – plant-wide model with MBR, chemical precipitation, closed loop DO controllers in the aerobic zones and NO_3 controller in the post-anoxic zone. For the DO controllers, the DO concentrations in the aerobic tanks were controlled to a set point of 2.0 $g.m^{-3}$ by manipulating the air supply rate, while an external carbon source was added to the post-anoxic tank to maintain the concentration of NO_3-N at 3 $gN.m^{-3}$ for the NO_3 controller.

ii) Scenario 2 *with step change in $FeSO_4$ dose*. This scenario determined the phosphorus response time constant under dynamic conditions with the calibrated plant-wide model, when the dosage of iron salts was changed (increased or decreased by 10%), to assess how this would affect phosphorus removal. The time constant was determined as the time required by the effluent P to reach 63.2% (from a 10% $FeSO_4$ step decrease or increase) of its total change.

iii) Scenario 3 *with phosphorus controller*. The base case was simulated as in Scenario 1 except for dosing of Fe salts, with a predefined concentration of phosphorus in the effluent being controlled by manipulating the dose flow rates ($FeSO_4$ or $FeCl_3$). This scenario examined whether inclusion of a phosphorus controller for chemical precipitation, would be essential to achieve low P effluent concentrations, whilst at the same time preventing detrimentally low P concentrations with adverse effects on biological processes in the bioreactors.

iv) Scenarios 4, 5 & 6 were designed to investigate the impact of changing dosing location for iron sulphate to the activated sludge system. During this simulation analysis, $FeSO_4$ addition was varied between three different locations, namely anoxic (BR1/ANOX), aerobic (BR4/AER), and RAS-deoxygenation (RASDEOX) compartments in Scenario 4, Scenario 5 and Scenario 6, respectively.

3 Results and discussion

3.1 Steady-state influent characteristics

Data from 2015 were used to fractionate COD and calculate COD ratios, which were obtained from the 2016-2017 data used in the steady-state simulations. Table 2 shows the measured total, filtered and flocculated COD data, as well as the various COD fractions obtained from the 2015 data. The readily biodegradable and fermentation products fractions accounted for 13% and 9% of total COD, respectively.

The slowly biodegradable fraction had the highest percentage (56% of total COD), while the non-biodegradable organics and the heterotrophic biomass represented 11% and 6% of total COD, respectively. The non-biodegradable fraction was used as one of the calibration parameters for sludge age in the activated sludge system; however, the effect of this parameter adjustment was outweighed by the separate effect of an adjusted primary clarifier efficiency influencing the amount of particulates entering the activated sludge system.

The averaged influent measurements and modelled influent composition for the pilot-plant are presented in Tables 3 and 4, respectively. The pilot-plant has limited COD data available and so the total organic carbon (TOC) measurements were converted to COD using an observed COD/TOC ratio of 3.5. The plant had a medium strength influent with respect to concentrations of organic matter (148 $gTOC.m^{-3}$; 521 $gCOD.m^{-3}$) and nutrients, such as ammonia nitrogen (37 $gN.m^{-3}$), and orthophosphate phosphorus (3.3 $gP.m^{-3}$). The influent contained 6.23 $g.m^{-3}$ of total phosphorus, of which about 53% was soluble phosphorus. Total nitrogen included 76% ammoniacal nitrogen, while the remainder was organic nitrogen. The raw wastewater influent contained 249 $gTSS.m^{-3}$ of total suspended solids (TSS), of which 86% was volatile and the remainder was inorganic.

Using the COD ratio described above, the estimated organic matter content included a significant quantity of soluble COD (174 $gCOD.m^{-3}$), including VFAs (40 $gCOD.m^{-3}$). The results of the characterization showed a low (0.15) ratio between the readily biodegradable and slowly biodegradable substrates. The ratio of inert organic matter to slowly biodegradable substrate was also 0.15. These ratios did not change substantially after the primary clarifier, because the clarifier was performing very poorly with a removal efficiency of less than 30% TSS.

3.2 Dynamic influent characteristics

Figure 1 shows a representative pilot-scale data set over 294 days from June 2016 to April 2017, together with the BSM2 influent generator model simulations for flow rate, COD, NH_4-N and PO_4-P. Simulation results were in reasonably good agreement with measured results in terms of concentrations of ammonia nitrogen, phosphate, COD and TSS. We note that the influent generator provided modelled data at 5 min intervals, whereas actual measurements were relatively sparse with only daily or weekly sampling and analysis. The representative influent file created by the BSM2 influent generator model was used for dynamic simulation analyses.

3.3 Plant steady-state results

3.3.1 Model calibration

Figure 2 presents the modelled steady state and average measured data for key variables. With the minimal parameter adjustments described in Section 2.6, it was possible to achieve good agreement between modelled and measured TSS, PO_4-P and NH_4-N in the different streams of the pilot-plant. Further, the model was able to confirm the observed concentration of P in the effluent. For the steady-state scenario, differences between measured and modelled phosphorus of 5-10% were observed throughout the pilot-plant, and the prediction error for ammonia nitrogen was low at below 1%. The relative error for measured and predicted suspended solids (SS) in the primary effluent, mixed liquor and return activated sludge was reasonable at 3%, 1% and 6%, respectively. However, significant SS differences were seen in the effluent, likely due to faulty SS meters in the pilot-plant. The model instead assumes ideal complete retention of solids, due to the presence of the membranes.

The total iron concentration was low in the effluent (0.12 $gFe.m^{-3}$), indicating that almost all of the added iron salts precipitated out of the mixed liquor and were incorporated into the activated sludge. Available data for iron speciation and the precipitation model were limited, nevertheless pilot-plant performance

with respect to final effluent concentration of total iron was predicted very reasonably. Given the low concentration of total Fe in the effluent, it could be assumed that dosing $FeCl_3$ at the membranes provided additional removal of P, with no evidence of short-circuiting of dissolved iron. As such, a large amount of iron minerals in the form of HFO (about 70% of iron precipitates) and iron phosphate (approximately 30% of iron precipitates) were retained in the activated sludge within the bioreactors, with the associated precipitation and adsorption most likely accounting for the phosphorus removal. The proportion of HFO/$FePO_4$ significantly varies depending on a number of operational factors, including sludge age, pH, Fe/P ratio, the transformation between Fe^{2+} and Fe^{3+}, and the equilibrium concentrations of ferric iron and soluble phosphate. These factors are vital when assessing control strategies with respect to efficient removal of phosphorus. While pilot-plant data related to Fe^{2+} and Fe^{3+} species were unavailable, a literature review shows that ferrous iron added to an oxidizing environment fully converts to ferric iron, which then participates in P removal via precipitation or adsorption pathways (Wang *et al.*, 2014). Whilst, the conversion of ferrous iron to ferric iron could be implemented as a simple instantaneous reaction, a fast kinetic approach was used instead in this modelling study, and did not compromise simulation speed. In general, dosing of Fe^{3+} may be preferred to avoid an oxidation step; however, this would depend on the relative cost of ferric and ferrous salts. In general, the study showed that iron speciation is key in studying Fe chemistry and will therefore increase understanding of chemical P removal mechanisms.

In terms of energy recovery, the model simulated biogas production at 2.4 $Nm^3.d^{-1}$, which is probably lower than expected due to the low sedimentation efficiency in the primary clarifier (less than 30%). However, experimental data were not available to confirm prediction accuracy, due to the lack of a dedicated sludge treatment train.

3.3.2 Impact of pH and Fe/P molar ratio

The calibrated plant-wide model was used to carry out further simulations to study the impact of pH and molar ratio of Fe/P on the removal efficiency of phosphorus. As shown in Figure 3, the effluent P

417 concentration substantially decreased with decreasing pH at all Fe/P molar ratios. For example, for the
418 lowest ratio (Fe/P=1), the effluent P dropped from 0.39 $gP.m^{-3}$ at higher pH (7.4) to 0.02 at pH 6.7.
419 However, the relative differences of P concentrations in the effluent between the highest and lowest Fe/P
420 ratios was higher (0.63) at higher pH but became smaller (0.09) at lower pH. This shows that the pH and
421 the molar ratio of iron to the phosphorus concentrations affect the competition between hydroxyl ions and
422 phosphates for ferric ions at the point of addition. These results are in good agreement with other studies
423 (Hauduc *et al.*, 2015). In general, the pH of a wastewater affects chemical species distribution of the weak
424 acid-base systems, such as phosphate, and ferric iron speciation, which in turn dictate simultaneous
425 chemical precipitation and adsorption. Furthermore, the results show that increasing the concentrations of
426 iron salts may not translate in further removal of phosphorus when residual P concentration is already
427 very low. This is in agreement with other studies, which have reported that the efficiency of dosed
428 chemicals declines significantly at low phosphorus concentrations (De Haas *et al.*, 2000a; 2001b).

429 ***3.4 Assessment of model dynamic responses***

430 3.4.1 Time constant of chemical precipitation

431 Figure 4 presents the results of simulations where a step change in the dose of $FeSO_4$ was introduced. The
432 time constants of the response of the P concentration were found to be 5.25 days and 5 days, when the
433 iron dose rate was decreased and increased by 10%, respectively. Therefore, when the dosing of $FeSO_4$ is
434 changed in the wastewater treatment system, the effluent P varies accordingly in a time-dependent
435 manner with slow dynamics. With the observed first-order response, the initial change in effluent P is
436 greatest, eventually levelling off at a new equilibrium state at least within about 5 days. The overall slow
437 response is likely the result of the complex multi-step process of dissolution, oxidation, formation, growth
438 and aging of HFO complexes, affecting phosphorus adsorption in a time-dependent manner in the model.

439 Similarly, the experimental investigations (shown in Figure S2) at the pilot-plant under study similarly
440 showed a slow response when the dosed amount of precipitants was changed, and therefore corroborate

441 these simulation results (Figure 4). The representation in the model (as seen in the simulation results)
442 induces a persistent effect of the dosed iron being recycled in the sludge and continuing to remove
443 phosphorus well after reducing/stopping the chemical dosing. Again, this was corroborated by actual
444 measurement observations in the pilot plant. Specifically, the model description includes chemical
445 phosphorus removal via two simultaneous reactions: a reaction of phosphate and HFO (by adsorption and
446 co-precipitation) as well as a rapid direct iron phosphate precipitation (possible at the point of chemical
447 addition) (Wu *et al.*, 2015). Freshly formed HFO and possibly (amorphous) iron phosphate in the
448 wastewater, are potentially highly reactive (high surface areas or many binding sites) and able to partake
449 in the removal of phosphorus from wastewater. However, reactivity of HFO deteriorates through ageing
450 that occurs as the minerals accumulate in the bioreactors and continues to be recycled as part of the RAS.
451 This indicates that the progressive accumulation of the Fe precipitates continuously facilitates additional
452 phosphorus removal. The implication of this assertion is that the solid retention time (SRT) plays a
453 critical role in determining the effluent P concentration. In other words, during simultaneous
454 precipitation, iron dosed directly to the bioreactors or membrane tanks within the MBR system, where
455 sludge recycling is taking place with much longer SRTs (23 days), will participate in P removal.
456 Additionally, the effluent P will decrease with increasing SRT, indicating that the sludge age is one of the
457 key operational parameters controlling the iron sludge content in the bioreactors and influences both the P
458 in the effluent and eventually the membrane characteristics. On the other hand, a higher SRT would
459 involve the potentially competing effect of accumulating older less reactive sludge. However, from pilot-
460 plant observations in this study, HFO reactivity is reasonably maintained, presumably by iron, cycling in
461 the MBR system, undergoing reduction-oxidation reactions whilst alternating between anoxic and aerobic
462 conditions (Bligh *et al.*, 2017). This is represented in the model.

463 3.4.2 Plant-wide dynamic results

464 In order to demonstrate the application of the plant-wide model, several scenarios were considered in
465 which effluent phosphorus concentrations around 0.05-0.4 $gP.m^{-3}$ were obtained, using a stoichiometric

466 molar ratio Fe/P = 2 with respect to the influent concentration. The effect of increasing or decreasing the
467 quantity of dosed chemicals was investigated as part of Scenario 2. The dosing chemicals ($FeSO_4$ and
468 $FeCl_3$) were fed directly to the aerobic tank and membrane tanks, respectively. Their concentrations were
469 decreased by 10% after 120 days while the plant was operated under dynamic conditions. Dosing $FeSO_4$
470 to the aerobic tank led to the oxidation of Fe^{3+}, which played a key role in removing P. Figure 5a displays
471 the total phosphorus in the influent, which is also compared to the total amounts of iron salt dosed at the
472 three dosing locations to remove phosphorus from the influent, as shown in Figure 5b, as well as the
473 concentration profile for phosphorus in the secondary effluent, as shown in Figure 5c. The striking feature
474 in controlling PO_4 in the effluent is that the total amount of added iron was reduced by 18% from 1046
475 $gFe.d^{-1}$ in Scenario 1 (PO_4 open loop) to 889 $gFe.d^{-1}$ in Scenario 3 (PO_4 closed loop). This reduction
476 clearly shows the benefits of controlling Fe dosage and how it could significantly impact the operational
477 cost of removing P from wastewater. It is worthwhile to mention that about 8.9% of the iron dosed in the
478 first scenario, was added as Fe^{3+}, while the remainder (91.1%) was dosed as $FeSO_4$. The overall amount
479 of Fe^{3+} was 8.6% in the second scenario, however, it increased significantly to 44.6% in Scenario 3 (see
480 Section 3.4.2 for further discussions). The simulation results in Figure 5c show that the concentrations of
481 phosphorus in the effluent increased by approximately 44% for the 2nd scenario and decreased by 15% for
482 the 3rd scenario, respectively. The increase of phosphorus in the effluent in the 2nd scenario is due to the
483 decreased contribution of the iron salt flows to the aerobic tank and membrane tanks.

484 Scenario 2 was carried out to simulate the behaviour of the pilot-plant if the $FeSO_4$ dosage had been less
485 than required for a significant period of time, and the control system takes corrective measures to ensure
486 that the effluent quality is maintained. For example, after a period of limited dosage (e.g. due to incorrect
487 concentration of precipitation chemicals), the modelling results (Figure 5c) showed that such scenarios
488 could be compensated for by increasing and decreasing subsequent Fe salt dosage in a controlled manner.
489 As indicated above, redox cycling of iron in an MBR system is expected to maintain or reduce the rate of
490 HFO reactivity loss as a result of reduction in anoxic zones and oxidation in aerobic zones (Blight *et al*.,

2017). To this end, the presence of the accumulated precipitates has a beneficial effect on phosphorus, and a major mechanism of phosphorus removal, likely due to the long contact time with the accumulated sludge leading to removal of P by adsorption or co-precipitation. The amount and reactivity of existing minerals present in the activated sludge are among the most influential factors for phosphorus removal by simultaneous precipitation adsorption reactions.

Figure 6 shows the results of concentration profiles of ammonia nitrogen in the secondary effluent for the first three scenarios combined. The simulation results indicate that the concentrations of ammonia nitrogen in the effluent decreased by approximately 8.7% for the 2nd scenario and decreased by 8.2% for the 3rd scenario, respectively. The spikes in the simulated ammonia concentrations corresponded very well to lower concentrations of soluble phosphate in the bioreactors. Overall, these results indicate that phosphorus deficiency due to simultaneous precipitation may be detrimental to autotrophic nitrifying bacteria, which require enough phosphorus for cell growth. It should be noted that a phosphorus limitation can occur when the concentration of phosphorus is in the range of 0.1 to 0.3 gP.m^{-3} (Metcalf & Eddy, 2004). This highlights the necessity to control the level of bioreactor phosphate concentrations to reduce the risk of biological processes being limited by low phosphate.

3.4.3 Impact of controlling iron salt ($FeSO_4$ & $FeCl_3$) dosing

The impact of imposing a basic control and operational strategy for maintaining the concentration of phosphate below a required future effluent standard, was investigated for demonstration purposes. The results in Figure 5c (Scenario 3) indicate that the implemented PO_4 control strategy, enabled the plant to reach P effluent concentrations of about 0.15 gP.m^{-3} as stipulated by the future effluent quality standard, whilst at the same time ensuring that the iron dosage was appropriate. However, the location of the two P controllers appeared to be an important factor for achieving minimum consumption of iron coagulants. For example, when the sensor for $FeSO_4$ dosage was at the same location (secondary effluent) as the one for $FeCl_3$ dosage, the simulation indicates that only the $FeCl_3$ controller with the lower set point (0.15

gP.m^{-3}) was effective. Moving the location of the $FeSO_4$ controller before the post-anoxic tank (at the outlet of the anoxic tank before addition of $FeCl_3$) led to a reduction of iron coagulant by 15% since both controllers were working as per set criteria. This is in agreement with the recommendations of Ingildsen & Olsson (2002), that sensors located in close proximity to the controlled processes are preferable for a good controller performance. Controlling Fe salts dosing also provides additional benefits of maintaining optimal conditions for nitrification/denitrification processes. It has been shown that biological nutrient removal mechanisms function less well in the presence of chemical precipitation, under conditions where the P concentration in the activated sludge is too low and potentially limiting (Philips *et al.*, 2015). Such conditions with low P may be prevalent in WWTPs with MBRs and chemical P removal, such as in the pilot-scale plant under study, designed to reach very low effluent P concentrations. Therefore, it is recommended to control the addition of iron salts. When the P controllers are maintained at their set points by closed-loop control, the simulations indicate that the WWTP will not only achieve lower P values in the effluent but also more efficient chemical use.

3.4.4 Impact of iron dosing location

To maximize the removal of phosphorus in the presence of iron salts, different iron dosing locations including the aerobic tank, anoxic tank and RASDEOX stream, were investigated. Given that the dissolved oxygen content of the RASDEOX stream from the membrane tanks is high and can have impact on the denitrification process in the anoxic tank, simulations were used to analyse whether adding Fe(II) salts in this location could provide additional benefits in reducing the oxygen level in the stream being recirculated to the activated sludge. Figure 7 shows the results of the simulated effluent P concentrations for the impact of $FeSO_4$ dosing at the three different locations in the activated sludge system for Scenarios 4, 5 and 6. The dosing location in each case was changed at the beginning of the simulation.

In comparison to Scenario 4 (default dosing location), the simulation results indicate that the concentrations of phosphorus in the effluent increased by roughly 17% and 13% for the 4th and 5th

539 scenarios, respectively. Whereas in the case of ammonia nitrogen concentration in the effluent, the
540 reduction is small: 0.96% in the 4th scenario and 1.8% in the 5th scenario. The decrease of nitrate in the
541 effluent in the fifth scenario is likely due to the decreased contribution of RASDEOX oxygen entering the
542 anoxic tank. In general, the results show that iron addition at these locations had a limited impact on
543 phosphorus removal performance. The implication would be that $FeSO_4$ dosing should be fed at an
544 aeration stage in the activated sludge process, where there is good mixing. When dosed prior to the
545 aeration tank, ferrous salts will dissolve and then some of the resulting Fe^{2+} will be oxidized to ferric iron
546 by nitrate (anoxic zone), whereas the remaining Fe^{2+} will undergo oxidation in the aerobic zone.

547 ***3.5. Discussion***

548 3.5.1 General description of P/Fe interactions in water treatment systems and singularity of the presented
549 research

550 The study summarized in this paper has gone beyond the state of the art mathematical modelling practice
551 with an approach accounting for P and Fe transformations in both water and sludge line. Simulation
552 results were validated with N, P, Fe and TSS measurements at different parts of the plant. As far as the
553 authors are aware, the work herein does not resemble any other study in the published literature. Previous
554 studies described Fe-P processes with lab-scale data (Hauduc *et al.*, 2015) or, when full-scale, only the
555 water line had been accounted for (de Haas 2000a; 2000b; 2001). Full-scale examples predicting P
556 dynamics, verified with experimental data, did not include the Fe component (Kazadi-Mbamba *et al.*,
557 2016). The latter has a strong effect on the overall process performance as shown by (Solon *et al.*, 2017)
558 and by the present study results.

559 3.5.2. Model based optimization for improved performance

560 The overall results of this study demonstrate an iron transformation and precipitation model as part of
561 plant-wide model is a suitable tool for assessing chemical P removal from activated sludge. The model

562 enabled the prediction of iron consumption and P effluent and could be used to develop control strategies
563 to optimize simultaneous precipitation in terms of chemicals consumption while maximizing nutrients
564 removal as far as stringent effluent discharge requirements are concerned. However, a complete
565 calibration and validation of an activated sludge model combined with chemical P removal requires
566 additional influent characterization of soluble chemical components, particularly iron species, to be
567 incorporated into the physico-chemical module. In general, wastewater utilities only carry out limited
568 routine measurements, which also include very limited measurements of soluble chemical components.
569 To increase the accuracy of predicting simultaneous precipitation, it would be essential to perform
570 additional measurements that cover other relevant components, especially non-typical wastewater
571 constituents (e.g. iron species) that play a significant role in modelling chemical P removal, but for which
572 there is currently limited knowledge.

573 The model analysis focused quite extensively on the fate of iron and phosphorus in the activated sludge
574 system. However, it should be pointed out that the plant-wide model used, included a sludge treatment
575 train which consisted of sludge thickening, digestion and dewatering. During anaerobic digestion of waste
576 activated sludge, iron is released as a result of HFO reduction and iron phosphate dissolution leading to
577 an increased soluble concentration of iron. Sludge digestion also produces sulphide due to sulphate
578 reduction and the degradation and reduction of sulphur-containing organics (Batstone *et al.*, 2002). The
579 produced sulphide preferentially binds with iron to form iron sulphide minerals leading to a low
580 concentration of dissolved sulphide and hence decreases H_2S concentration in the biogas phase (Ge *et al.*,
581 2013). Therefore, the model also has the potential to evaluate chemical dosing in anaerobic digesters for
582 hydrogen sulphide removal from biogas.

583

4 Conclusions

The present study demonstrates that an integrated model (ASM2d, ADM1, physico-chemical model) is suitable to account for biological nutrient and chemical P removal through Fe precipitation. The integrated model gave good results (representative of reality) when validated against the pilot-scale measurement data. The following were key modelling outcomes:

1) The plant-wide model was able to replicate with acceptable accuracy the trends in effluent soluble ammonia (1%), phosphate (5-10%) and suspended solids (1-6%) under steady-state.
2) Simultaneous precipitation of $FePO_4$ and HFO particulates including adsorption of P on HFO sites were the main mechanisms for phosphorus removal in the MBR system.
3) The simulations confirmed that the modelling approach was valid, particularly the dependency on pH, which showed a strong expected effect. The ratio of Fe/P was also identified as influential, which should be set (where possible) based on an effluent P target. At higher ratios, lower P concentrations are expected in the effluent. However, when the P concentration in the mixed liquor is very low (<0.2 $mgP.L^{-1}$), an increasing Fe/P ratio does not translate linearly into further removal of P.
4) When the P controllers were maintained at their set points by closed-loop control of the iron salts dose, the WWTP achieved lower P values in the effluent. Accordingly, it is recommended to control the addition of iron salts, which would normally also have a positive impact on the operational cost of P removal in wastewater.
5) The time constant of simultaneous precipitation in the calibrated model, in response to step change increase or decrease in $FeSO_4$ dose, was found to be roughly 5 days. This indicated a slow dynamic response, likely due to multiple steps of dissolution, oxidation, precipitation, aging, adsorption and co-precipitation processes.
6) The dosing point of $FeSO_4$ in the activated sludge system was analysed for three different locations: aerobic, anoxic and RASDEOX tanks. Dosing at the aerobic tank had a slightly higher

609 effect on the chemical P removal. Locations with high DO and good mixing conditions are
610 considered to be preferable for $FeSO_4$ addition due to fast oxidation of Fe^{2+} to Fe^{3+}.

611

612 # References

613 APHA (2012). Standard methods for the examination of water and wastewater. American Public Health
614 Association, Washington DC, USA.

615 Andersson, S., Ek, P., Berg, M., Grundestam, J., & Lindblom, E. (2016). Extension of two large
616 wastewater treatment plants in Stockholm using membrane technology. *Water Practice and*
617 *Technology*, *11*(4), 744-753.

618 Bertanza, G., Canato, M., Laera, G., Vaccari, M., Svanström, M., & Heimersson, S. (2017). A
619 comparison between two full-scale MBR and CAS municipal wastewater treatment plants: Techno-
620 economic-environmental assessment. *Environmental Science Pollution Research*, *24*(11), 17383-17393.

621 Bligh, M.W., Maheshwari, P., & David Waite, T. (2017). Formation, reactivity and aging of amorphous
622 ferric oxides in the presence of model and membrane bioreactor derived organics. *Water Research, 124*,
623 341-352.

624 Batstone, D.J., Keller, J., Kalyuzhnyi, S.V., Pavlostathis, S.G., Rozzi, A., Sanders, W.T.M., Siegrist, H.,
625 & Vavilin, V.A. (2002). Anaerobic Digestion Model No. 1. IWA Publishing, London, UK.

626 Daigger, G.T., Crawford, G.V., & Johnson, B.R. (2010). Full-scale assessment of the nutrient removal
627 capabilities of membrane bioreactors. *Water Environment Research*, *82*(9), 806-818.

628 De Haas, D.W., Ekama, G.A., & Wentzel, M.C. (2000a). The use of simultaneous chemical precipitation
629 in modified activated sludge systems exhibiting biological excess phosphate removal – Part 1: Literature
630 review. *Water SA*, *26*(4), 439-452.

631 De Haas, D.W., Ekama, G.A., & Wentzel, M.C. (2000b). The use of simultaneous chemical precipitation
632 in modified activated sludge systems exhibiting biological excess phosphate removal – Part 4:
633 Experimental periods using ferric chloride. *Water SA, 26*(4), 485-504.

634 De Haas, D.W., Wentzel, M.C., & Ekama, G.A. (2001). The use of simultaneous chemical precipitation
635 in modified activated sludge systems exhibiting biological excess phosphate removal: Part 5:
636 Experimental periods using a ferrous-ferric chloride blend. *Water SA, 27*(2), 117-134.

637 Ekama, G.A. (2010). The role and control of sludge age in biological nutrient removal activated sludge
638 systems. *Water Science and Technology, 61*(7), 1645-1652.

639 Ekama, G.A., & Wenzel, M.C. (2004). A predictive model for the reactor inorganic suspended solids
640 concentration in activated sludge systems. *Water Research, 38*(19), 4093-4106.

641 EPA (Environmental Protection Agency) (2010). Nutrient Control Design Manual, State of Technology.
642 The Cadmus Group Inc., USA.

643 Flores-Alsina, X., Kazadi Mbamba, C., Solon, K., Vrecko, D., Tait, S., Batstone, D.J., Jeppsson, U., &
644 Gernaey, K.V. (2015). A plant-wide aqueous phase chemistry module describing pH variations and ion
645 speciation/pairing in wastewater treatment process models. *Water Research, 85*, 255-265.

646 Flores-Alsina, X., Saagi, R., Lindblom, E., Thirsing, C., Thornberg, D., Gernaey, K.V., & Jeppsson, U.
647 (2014). Calibration and validation of a phenomenological influent pollutant disturbance scenario
648 generator using full-scale data. *Water Research, 51*(15) 172-185.

649 Flores-Alsina, X., Solon, K., Kazadi Mbamba, C., Tait, S., Gernaey, K.V., Jeppsson, U., & Batstone, D.J.
650 (2016). Modelling phosphorus (P), sulfur (S) and iron (Fe) interactions during dynamic simulations of
651 anaerobic digestion processes. *Water Research, 95*, 370-382.

652 Frossard, E., Bauer, J.P., & Lothe, F. (1997). Evidence of vivianite in $FeSO_4$-flocculated sludges. *Water*
653 *Research, 31*(10), 2449-2454.

654 Ge, H., Zhang, L., Batstone, D., Keller, J., & Yuan, Z. (2013). Impact of iron salt dosage to sewers on
655 downstream anaerobic sludge digesters: Sulfide control and methane production. *Journal of*
656 *Environmental Engineering, 139*(4), 594-601.

657 Gernaey, K.V., Flores-Alsina, X., Rosen, C., Benedetti, L., & Jeppsson, U. (2011). Dynamic influent
658 pollutant disturbance scenario generation using a phenomenological modelling approach. *Environmental*
659 *Modelling & Software, 26*(11), 1255-1267.

660 Gernaey, K.V., Jeppsson, U., Vanrolleghem, P.A., & Copp, J.B. (2014). Benchmarking of control
661 strategies for wastewater treatment plants. IWA Publishing, London, UK.

662 Hauduc, H., Takács, I., Smith, S., Szabo, A., Murthy, S., Daigger, G.T., & Spérandio, M. (2015). A
663 dynamic physicochemical model for chemical phosphorus removal. *Water Research, 73*, 157-170.

664 Henze, M., Gujer, W., Mino, T., & van Loosdrecht, M.C.M. (2000). Activated sludge models ASM1,
665 ASM2, ASM2d and ASM3. IWA Publishing, London, UK.

666 Henze, M., Gujer, W., Mino, T., Matsuo, T., Wentzel, M., & Marais, G.v.R. (1995). Wastewater and
667 biomass characterization for the Activated Sludge Model No. 2: Biological phosphorus removal. *Water*
668 *Science and Technology, 31*(2), 13-23.

669 Henze, M., Harremoës, P., la Cour Jansen, J., & Arvin, E. (2002). Wastewater Treatment: Biological and
670 Chemical Processes. Springer, Berlin, Germany.

671 Ingildsen, P., & Olsson, G. (2002). Exploiting online in-situ ammonium, nitrate and phosphate sensors in
672 full-scale wastewater plant operation. *2nd World Water Congress: Wastewater Treatment and Sludge*
673 *Management, 46*(4-6), 139-147.

674 Jeppsson, U., Pons, M.N., Nopens, I., Alex, J., Copp, J.B., Gernaey, K.V., Rosen, C., Steyer, J.P., &
675 Vanrolleghem, P.A. (2007). Benchmark Simulation Model No 2: General protocol and exploratory case
676 studies. *Water Science and Technology, 56*(8), 67-78.

677 Judd, S. (2008). The status of membrane bioreactor technology. *Trends in Biotechnology*, *26*(2), 109-116.

678 Kazadi Mbamba, C., Batstone, D.J., Flores-Alsina, X., & Tait, S. (2015a). A generalised chemical
679 precipitation modelling approach in wastewater treatment applied to calcite. *Water Research, 68*, 342-
680 353.

681 Kazadi Mbamba, C., Tait, S., Flores-Alsina, X., & Batstone, D.J. (2015b). A systematic study of multiple
682 minerals precipitation modelling in wastewater treatment. *Water Research, 85*, 359-370.

683 Kazadi Mbamba, K., Flores-Alsina, X., Batstone, D.J., & Tait, S. (2016). Validation of a plant-wide
684 phosphorus modelling approach with minerals precipitation in a full-scale WWTP. *Water Research*, *100*,
685 169-183.

686 Metcalf & Eddy (2004). Wastewater Engineering: Treatment and Reuse (Tchobanoglous, G., Burton, F.
687 and Stensel, H. D., Eds., 4th ed.). McGraw-Hill, Boston, USA.

688 Nopens, I., Batstone, D.J., Copp, J.B., Jeppsson, U., Volcke, E., Alex, J. and Vanrolleghem, P.A. (2009)
689 An ASM/ADM model interface for dynamic plant-wide simulation. *Water Research*, *43*(7), 1913-1923.

690 Otterpohl, R., & Freund, M. (1992). Dynamic models for clarifiers of activated sludge plants with dry and
691 wet weather flows. *Water Science and Technology, 26*(5-6), 1391-1400.

692 Philips, S., Rabaey, K., & Verstraete, W. (2003). Impact of iron salts on activated sludge and interaction
693 with nitrite or nitrate. *Bioresource Technology*, *88*(3), 229-239.

694 Roeleveld, P., van Loosdrecht, M.C.M., & Henze, M. (2002). Experience with guidelines for wastewater
695 characterisation in The Netherlands. Water Science & Technology, 45(6), 77-87.

696 Solon, K. (2017). Extending wastewater treatment process models for phosphorus removal and recovery –
697 A framework for plant-wide modelling of phosphorus, sulfur and iron. PhD thesis, Division of Industrial
698 Electrical Engineering and Automation, Lund University, Sweden.

699 Solon, K., Flores-Alsina, X., Mbamba, C.K., Ikumi, D., Volcke, E.I.P., Vaneeckhaute, C., Ekama, G.,
700 Vanrolleghem, P.A., Batstone, D.J., Gernaey, K.V., & Jeppsson, U. (2017). Plant-wide modelling of
701 phosphorus transformations in wastewater treatment systems: Impacts of control and operational
702 strategies. *Water Research*, *113*, 97-110.

703 Smith, S., Takács, I., Murthy, S., Daigger, G.T., & Szabó, A. (2008). Phosphate Complexation Model and
704 Its Implications for Chemical Phosphorus Removal. *Water Environment Research*, *80*(5), 428-438.

705 Stumm, W., & Morgan, J.J. (1996). Aquatic chemistry: Chemical equilibria and rates in natural waters.
706 Wiley, New York, USA.

707 SUMO (2018). http://www.dynamita.com/the-sumo/

708 Wang, Y., Tng, K.H., Wu, H., Leslie, G., & Waite, T.D. (2014). Removal of phosphorus from
709 wastewaters using ferrous salts – A pilot scale membrane bioreactor study. *Water Research*, *57*, 140-150.

710 Wilfert, P., Mandalidis, A., Dugulan, A.I., Goubitz, K., Korving, L., Temmink, H, Witkamp, G.J., & van
711 Loosdrecht, M.C.M. (2016). Vivianite as an important iron phosphate precipitate in sewage treatment
712 plants. *Water Research*, *104*, 449-460.

713 Wu, H., Ikeda-Ohno, A., Wang, Y., & Waite, T.D. (2015). Iron and phosphorus speciation in Fe-
714 conditioned membrane bioreactor activated sludge. *Water Research*, *76*, 213-226.

715

716

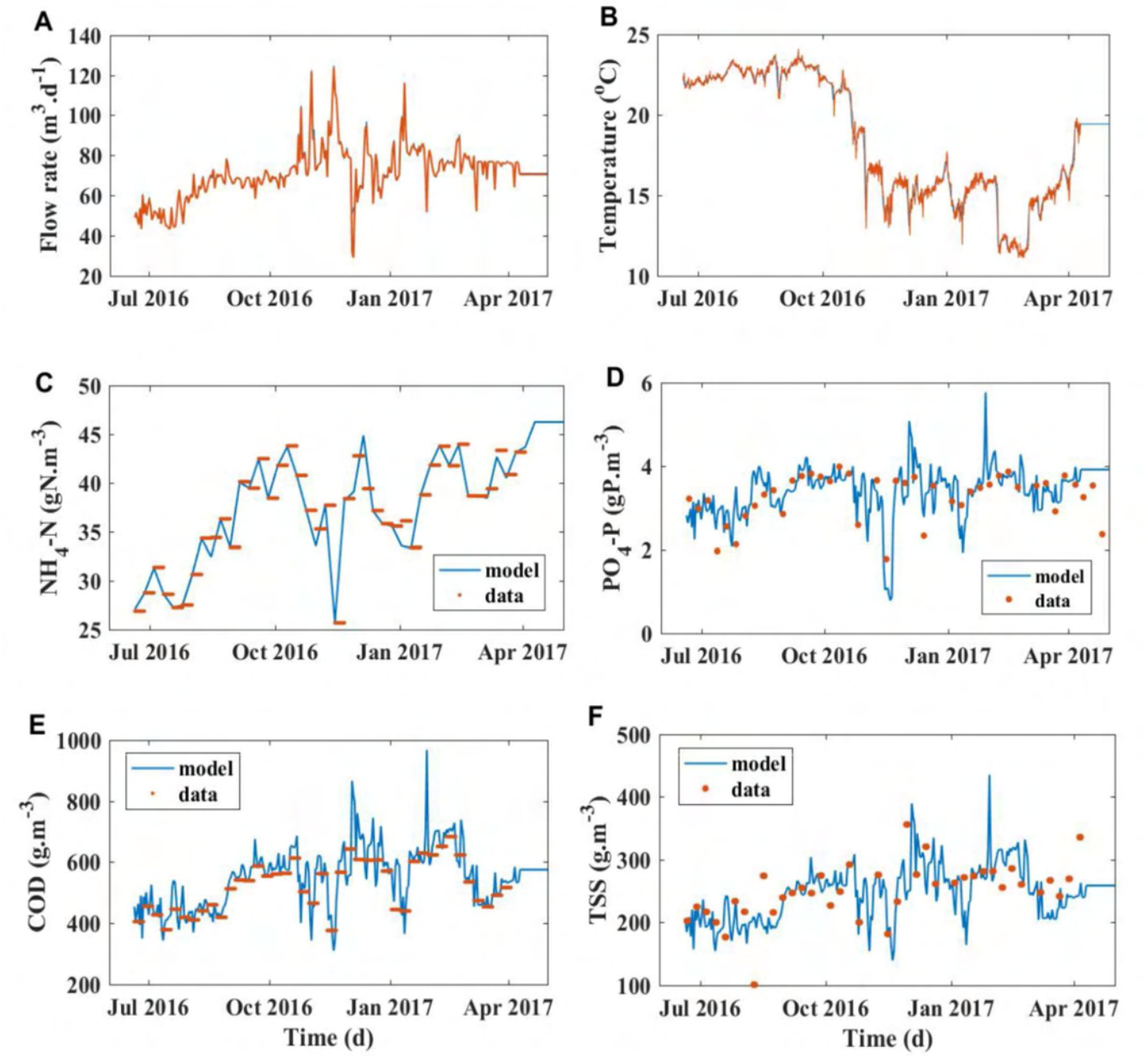

717

718 ***Figure 1*** *– Dynamic plant influent for representative measured and simulation data. The blue and red*

719 *solid lines represent the measured and simulated results, respectively.*

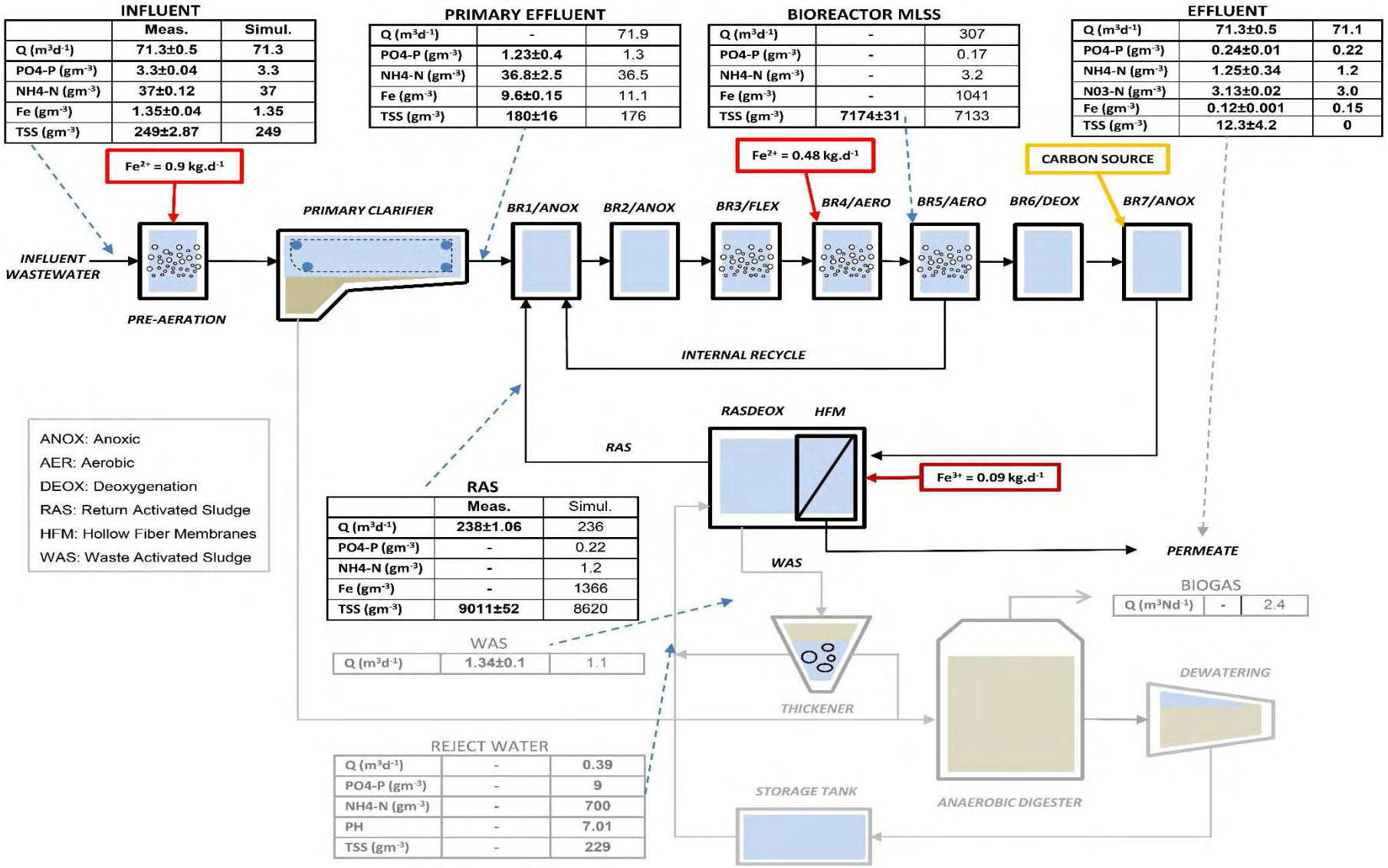
INFLUENT
Meas. Simul.
Q (m³d⁻¹) 71.3±0.5 71.3
PO4-P (gm⁻³) 3.3±0.04 3.3
NH4-N (gm⁻³) 37±0.12 37
Fe (gm⁻³) 1.35±0.04 1.35
TSS (gm⁻³) 249±2.87 249
PRIMARY EFFLUENT
Q (m³d⁻¹) - 71.9
PO4-P (gm⁻³) 1.23±0.4 1.3
NH4-N (gm⁻³) 36.8±2.5 36.5
Fe (gm⁻³) 9.6±0.15 11.1
TSS (gm⁻³) 180±16 176
BIOREACTOR MLSS
Q (m³d⁻¹) - 307
PO4-P (gm⁻³) - 0.17
NH4-N (gm⁻³) - 3.2
Fe (gm⁻³) - 1041
TSS (gm⁻³) 7174±31 7133
EFFLUENT
Q (m³d⁻¹) 71.3±0.5 71.1
PO4-P (gm⁻³) 0.24±0.01 0.22
NH4-N (gm⁻³) 1.25±0.34 1.2
N03-N (gm⁻³) 3.13±0.02 3.0
Fe (gm⁻³) 0.12±0.001 0.15
TSS (gm⁻³) 12.3±4.2 0
Fe2+ = 0.9 kg.d-1
Fe2+ = 0.48 kg.d-1
CARBON SOURCE
INFLUENT WASTEWATER
PRE-AERATION
PRIMARY CLARIFIER
BR1/ANOX
BR2/ANOX
BR3/FLEX
BR4/AERO
BR5/AERO
BR6/DEOX
BR7/ANOX
INTERNAL RECYCLE
RASDEOX
HFM
RAS
Fe3+ = 0.09 kg.d-1
PERMEATE
WAS
ANOX: Anoxic
AER: Aerobic
DEOX: Deoxygenation
RAS: Return Activated Sludge
HFM: Hollow Fiber Membranes
WAS: Waste Activated Sludge
RAS
Meas. Simul.
Q (m³d⁻¹) 238±1.06 236
PO4-P (gm⁻³) - 0.22
NH4-N (gm⁻³) - 1.2
Fe (gm⁻³) - 1366
TSS (gm⁻³) 9011±52 8620
WAS
Q (m³d⁻¹) 1.34±0.1 1.1
BIOGAS
Q (m³Nd⁻¹) - 2.4
THICKENER
DEWATERING
ANAEROBIC DIGESTER
STORAGE TANK
REJECT WATER
Q (m³d⁻¹) - 0.39
PO4-P (gm⁻³) - 9
NH4-N (gm⁻³) - 700
PH - 7.01
TSS (gm⁻³) - 229

Figure 2 *– Steady-state comparison between the model prediction and measured data for representative streams and variables across the pilot treatment plant.* $FePO_4$ *was added in a pre-aeration tank (before primary settling tank, not shown) and in the first aerobic tank,* $FeCl_3$ *was added before the MBRs.*

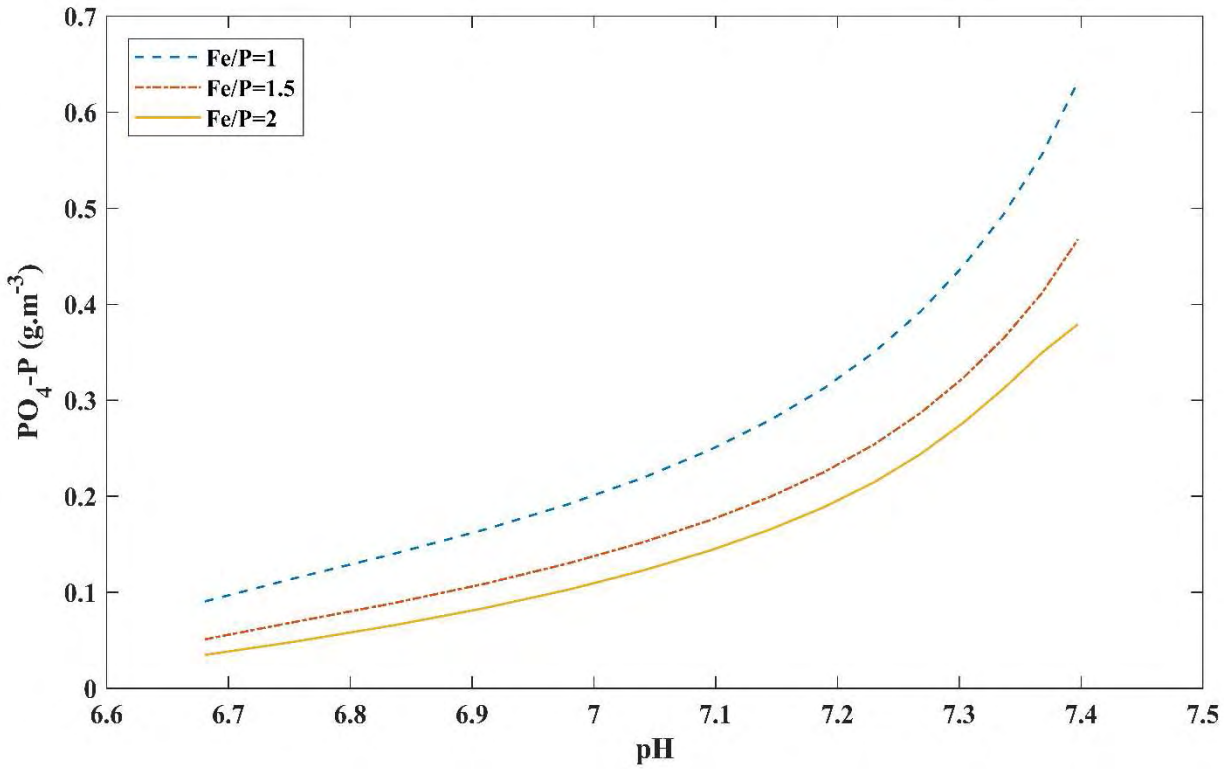

Figure 3 *– The impact of pH and Fe/P molar ratio on the dissolved phosphorus in the effluent.*

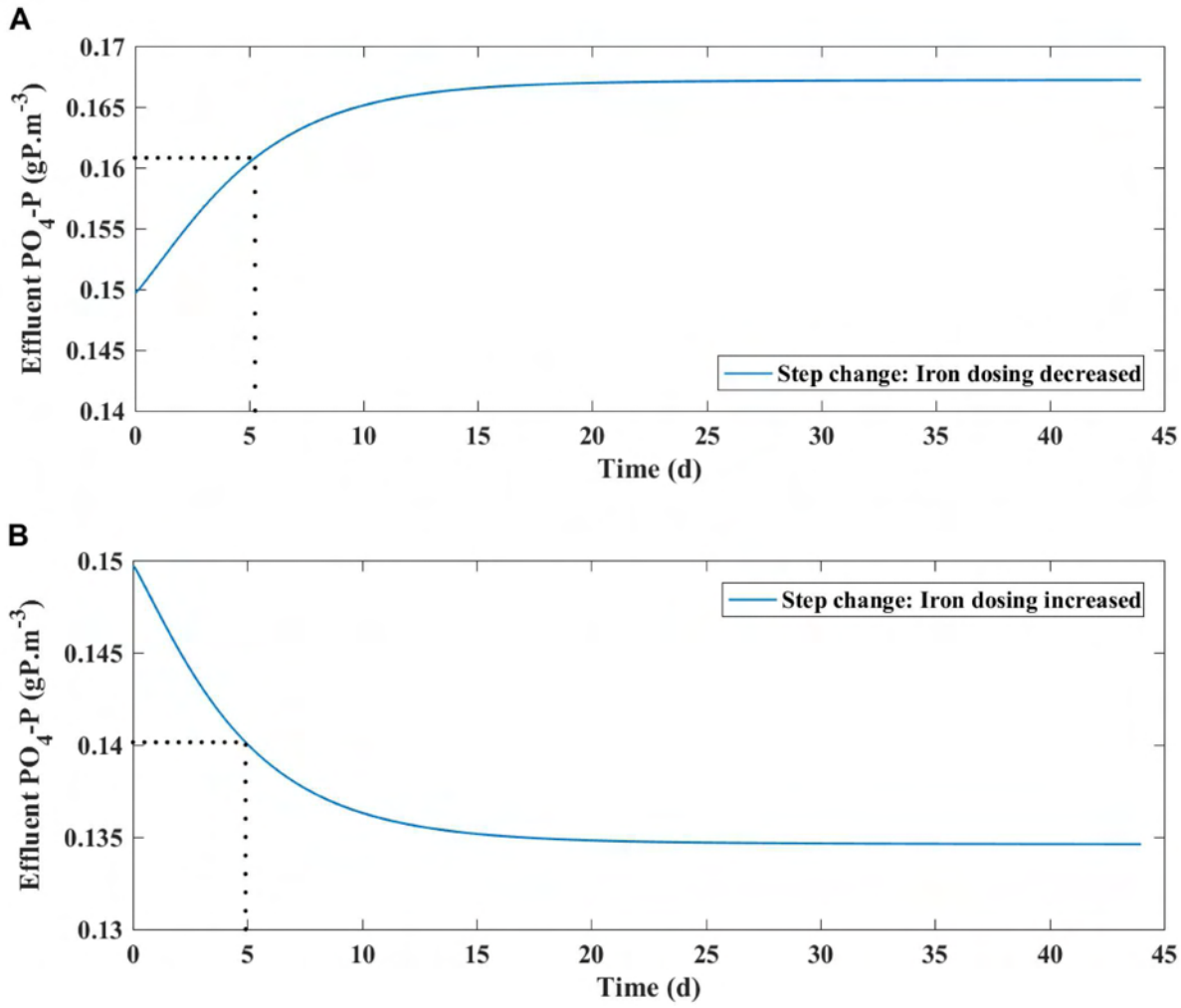

Figure 4 – *Dynamic response in effluent P to step change in iron salt ($FeSO_4$) dosage decrease (a) and increase (b).*

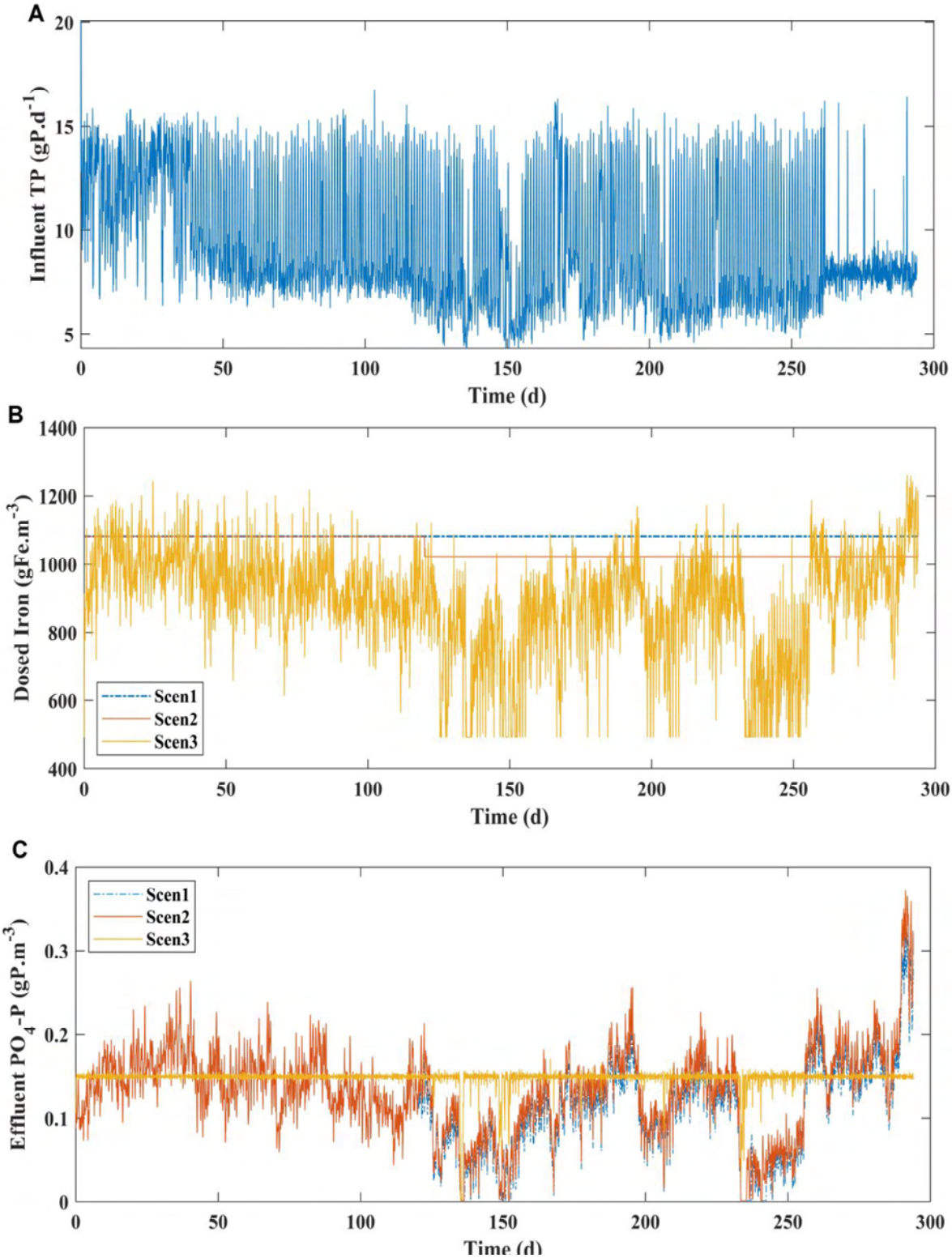

Figure 5 *– Total phosphorus in the influent (a), total amount of added iron ($FeSO_4$ and $FeCl_3$) at the three dosing locations for Scenarios 1 – 3 (b) and dynamic simulations of the soluble phosphate in the treatment plant outflow for Scenarios 1 – 3 (c).*

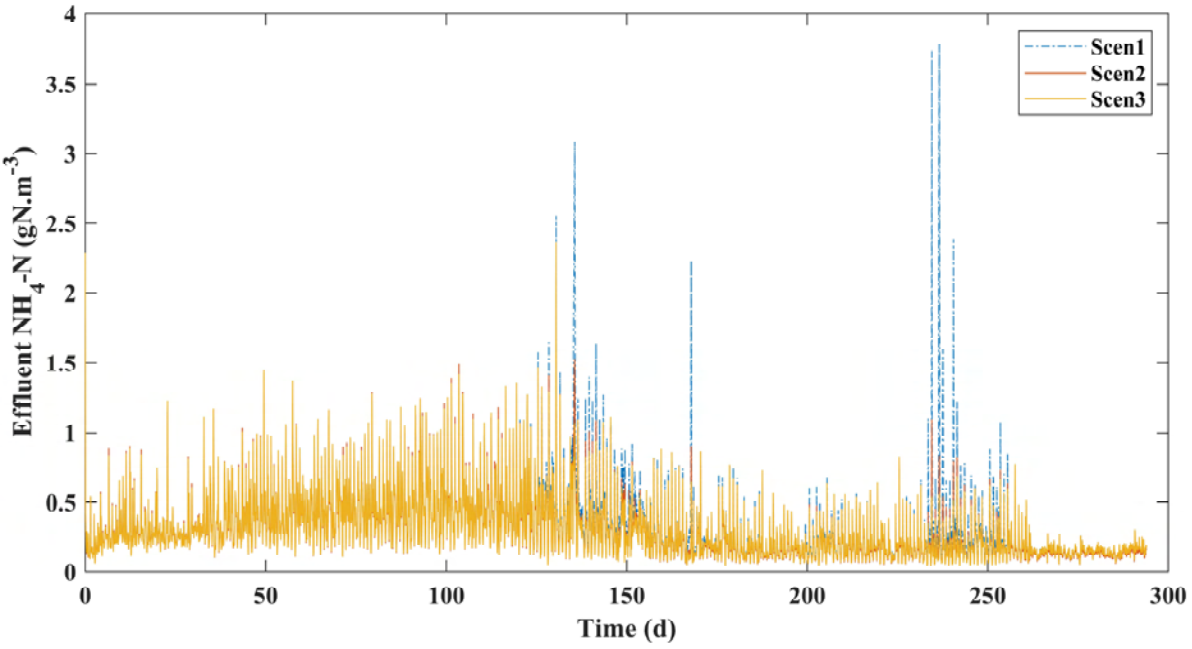

Figure 6 *– Dynamic simulations of ammonia nitrogen in the treatment plant outflow for Scenarios 1 - 3.*

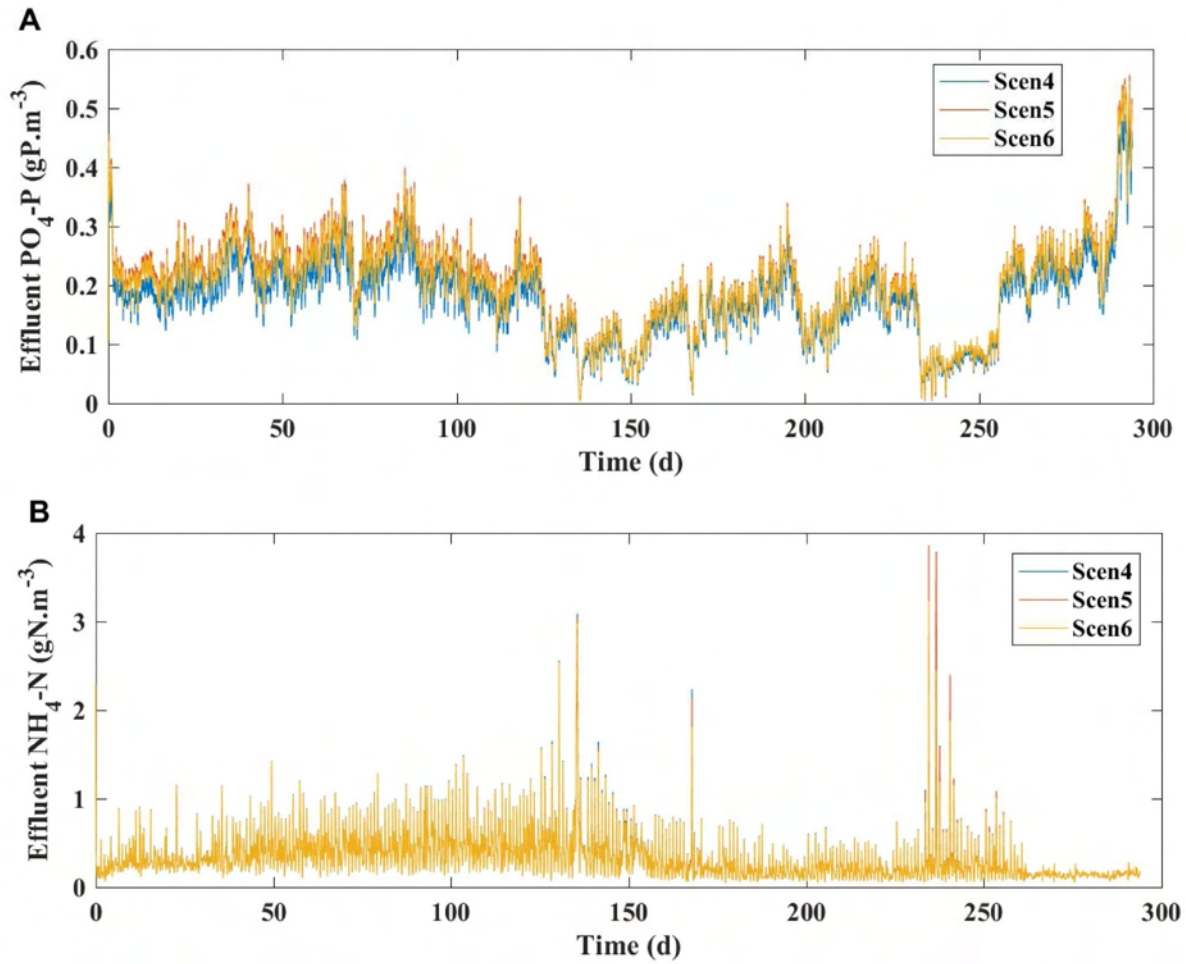

Figure 7 *– Dynamic simulations of the soluble phosphate and ammonia nitrogen in the treatment plant outflow for Scenarios 4, 5 and 6. The blue solid, red solid and yellow solid lines show the simulation results for the Scenario 4, Scenario 5 and the Scenario 6, respectively.*

Table 1 *– Composition of the supernatant from the full-scale anaerobic digesters at Henriksdal WWTP.*

Parameters	**Values**
Total COD ($gCOD.m^{-3}$)	502
Soluble COD ($gCOD.m^{-3}$)	337
Total nitrogen ($gN.m^{-3}$)	523
Ammoniacal nitrogen ($gN.m^{-3}$)	460
Total phosphorus ($gP.m^{-3}$)	18.2
Orthophosphate phosphorus ($gP.m^{-3}$)	1.60
Total iron ($gFe.m^{-3}$)	1.10
Total suspended solids ($gSS.m^{-3}$)	1560

Table 2 *– Measured total, filtered and flocculated COD for the 2015data, as well as COD fractions calculated and retained for the 2016/2017 data.*

Parameters	**COD (g.m^{-3})**	**COD ratio**
COD	466±42	1
Soluble COD	174±9	0.4
Flocculated COD	122±9	0.26
Readily biodegradable, S_F	60	0.13
Fermentation products, S_A	40	0.09
Inert biodegradable organics, S_I	22	0.05
Non-biodegradable organics, X_I	61	0.11
Slowly biodegradable substrate, X_S	245	0.56
Heterotrophic biomass, X_H	38	0.06
Autotrophic biomass, X_{AUT}	0	0

Table 3 *– Average steady-state influent composition of the pilot-scale WWTP used for influent characterization (2016/2017 data)*

Parameters	**Measurements**
Total COD ($gCOD.m^{-3}$)	521
Soluble COD ($gCOD.m^{-3}$)	174
Flocculated COD ($gCOD.m^{-3}$)	137
BOD_7 ($gCOD.m^{-3}$)	234
TN ($gN.m^{-3}$)	48
Ammoniacal nitrogen NH_4 ($gN.m^{-3}$)	37
Nitrate, NO_x ($gN.m^{-3}$)	0.12
Total phosphorus, Ptot ($gP.m^{-3}$)	6.23
Orthophosphate phosphorus ($gP.m^{-3}$)	3.3
Total organic carbon, TOC ($g.m^{-3}$)	141
Total inorganic carbon, TIC ($g.m^{-3}$)	75
Total suspended solids, TSS ($gTSS.m^{-3}$)	249
Volatile suspended solids, VSS ($gVSS.m^{-3}$)	223
VFA ($gCOD.m^{-3}$)	40

Table 4 *– Average steady-state influent composition of the pilot scale WWTP used for influent steady state model validation. COD ratios determined previously was used for the influent composition.*

Model influent composition (ASM2d variables)	**Values**
Dissolved oxygen, S_{O2} ($g.m^{-3}$)	0
Readily biodegradable, S_F ($gCOD.m^{-3}$)	67
Fermentation products (acetate), S_A ($gCOD.m^{-3}$)	45
Ammoniacal nitrogen, S_{NH4} ($gN.m^{-3}$)	37
Nitrate (plus nitrite), S_{NO3} ($gN.m^{-3}$)	0.12
Phosphate, S_{PO4} ($gP.m^{-3}$)	3.3
Inorganic carbon, S_{IC} ($gC.m^{-3}$)	75
Inert biodegradable organics, S_I ($gCOD.m^{-3}$)	25
Inert non-biodegradable organics, X_I ($gCOD.m^{-3}$)	47
Slowly biodegradable substrate, X_S ($gCOD.m^{-3}$)	314
Heterotrophic biomass, X_H ($gCOD.m^{-3}$)	24
Volatile suspended solids, X_{VSS} ($g.m^{-3}$)	223
Inorganic suspended solids, X_{ISS} ($g.m^{-3}$)	26

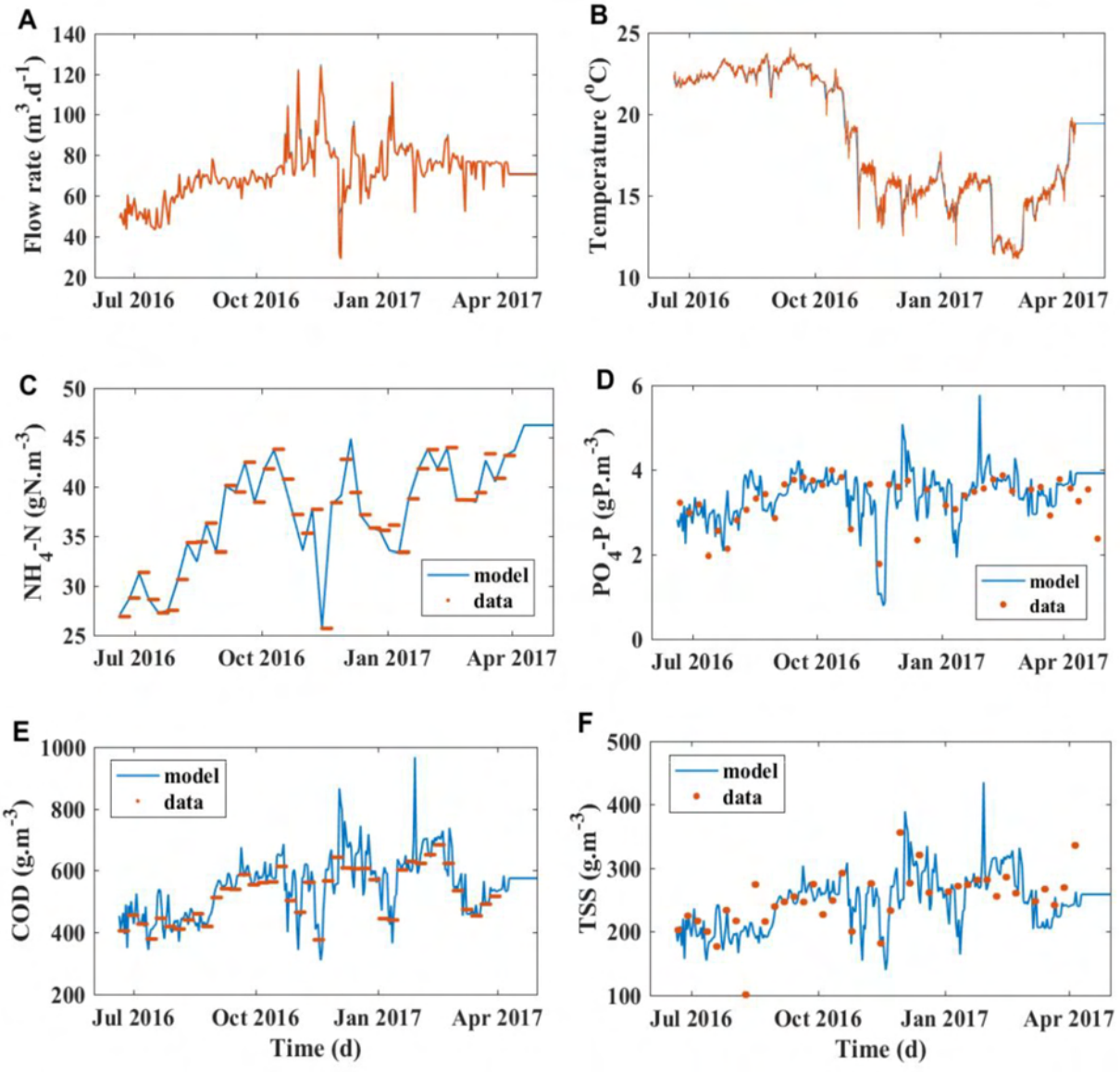
A
Flow rate ($m^3.d^{-1}$)
140
120
100
80
60
40
20
Jul 2016
Oct 2016
Jan 2017
Apr 2017
B
Temperature (^oC)
25
20
15
10
C
NH_4-N ($gN.m^{-3}$)
50
45
40
35
30
25
model
data
D
PO_4-P ($gP.m^{-3}$)
6
4
2
0
E
COD ($g.m^{-3}$)
1000
800
600
400
200
Time (d)
F
TSS ($g.m^{-3}$)
500
400
300
200
100

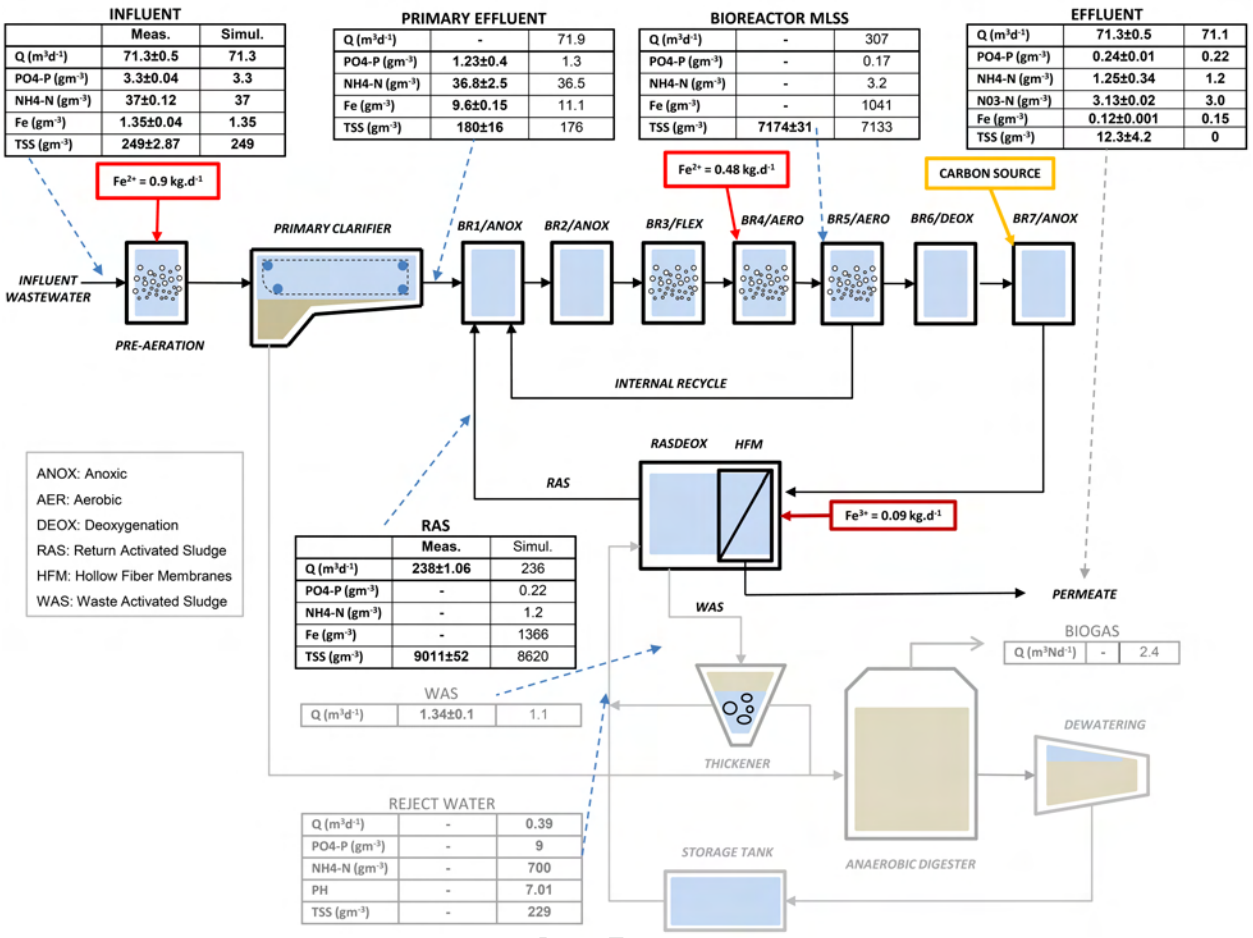
INFLUENT
Meas. Simul.
Q (m³d⁻¹) 71.3±0.5 71.3
PO4-P (gm⁻³) 3.3±0.04 3.3
NH4-N (gm⁻³) 37±0.12 37
Fe (gm⁻³) 1.35±0.04 1.35
TSS (gm⁻³) 249±2.87 249
PRIMARY EFFLUENT
Q (m³d⁻¹) - 71.9
PO4-P (gm⁻³) 1.23±0.4 1.3
NH4-N (gm⁻³) 36.8±2.5 36.5
Fe (gm⁻³) 9.6±0.15 11.1
TSS (gm⁻³) 180±16 176
BIOREACTOR MLSS
Q (m³d⁻¹) - 307
PO4-P (gm⁻³) - 0.17
NH4-N (gm⁻³) - 3.2
Fe (gm⁻³) - 1041
TSS (gm⁻³) 7174±31 7133
EFFLUENT
Q (m³d⁻¹) 71.3±0.5 71.1
PO4-P (gm⁻³) 0.24±0.01 0.22
NH4-N (gm⁻³) 1.25±0.34 1.2
N03-N (gm⁻³) 3.13±0.02 3.0
Fe (gm⁻³) 0.12±0.001 0.15
TSS (gm⁻³) 12.3±4.2 0
Fe2+ = 0.9 kg.d-1
Fe2+ = 0.48 kg.d-1
CARBON SOURCE
INFLUENT WASTEWATER
PRE-AERATION
PRIMARY CLARIFIER
BR1/ANOX
BR2/ANOX
BR3/FLEX
BR4/AERO
BR5/AERO
BR6/DEOX
BR7/ANOX
INTERNAL RECYCLE
RASDEOX
HFM
RAS
Fe3+ = 0.09 kg.d-1
PERMEATE
WAS
ANOX: Anoxic
AER: Aerobic
DEOX: Deoxygenation
RAS: Return Activated Sludge
HFM: Hollow Fiber Membranes
WAS: Waste Activated Sludge
RAS
Meas. Simul.
Q (m³d⁻¹) 238±1.06 236
PO4-P (gm⁻³) - 0.22
NH4-N (gm⁻³) - 1.2
Fe (gm⁻³) - 1366
TSS (gm⁻³) 9011±52 8620
WAS
Q (m³d⁻¹) 1.34±0.1 1.1
BIOGAS
Q (m³Nd⁻¹) - 2.4
THICKENER
DEWATERING
REJECT WATER
Q (m³d⁻¹) - 0.39
PO4-P (gm⁻³) - 9
NH4-N (gm⁻³) - 700
PH - 7.01
TSS (gm⁻³) - 229
STORAGE TANK
ANAEROBIC DIGESTER

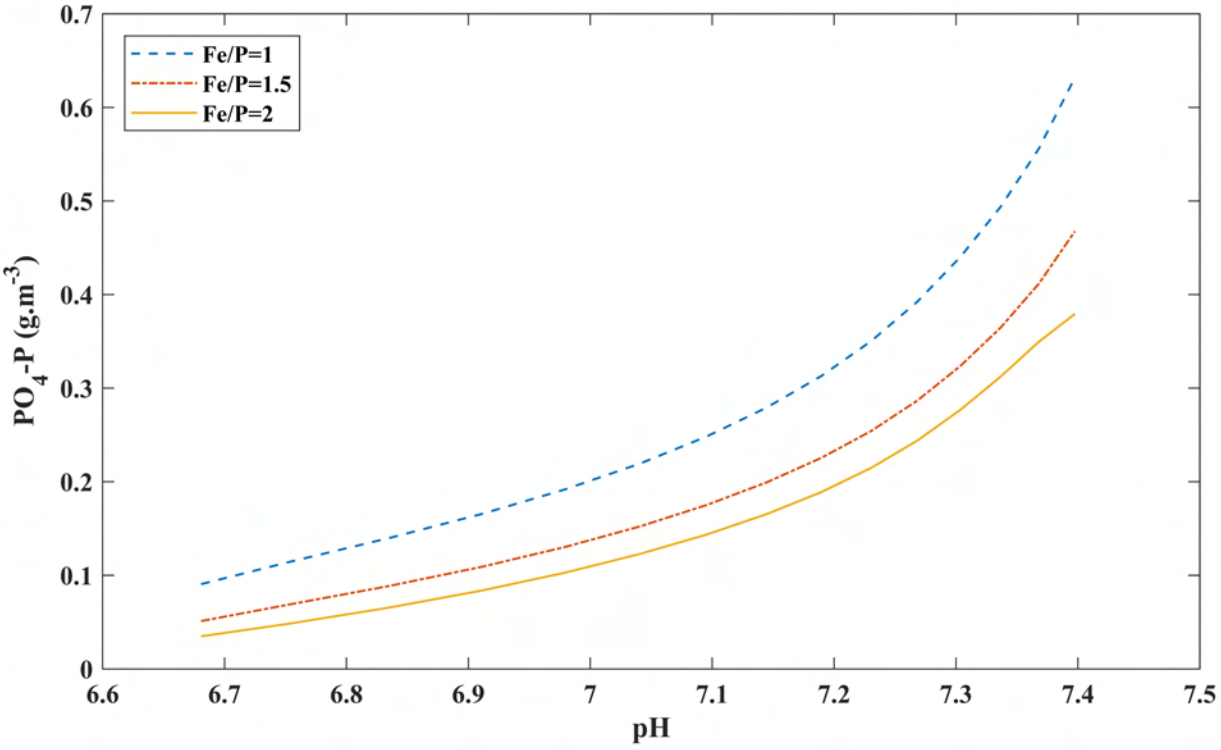
Fe/P=1
Fe/P=1.5
Fe/P=2
PO_4-P ($g.m^{-3}$)
pH
0
0.1
0.2
0.3
0.4
0.5
0.6
0.7
6.6
6.7
6.8
6.9
7
7.1
7.2
7.3
7.4
7.5

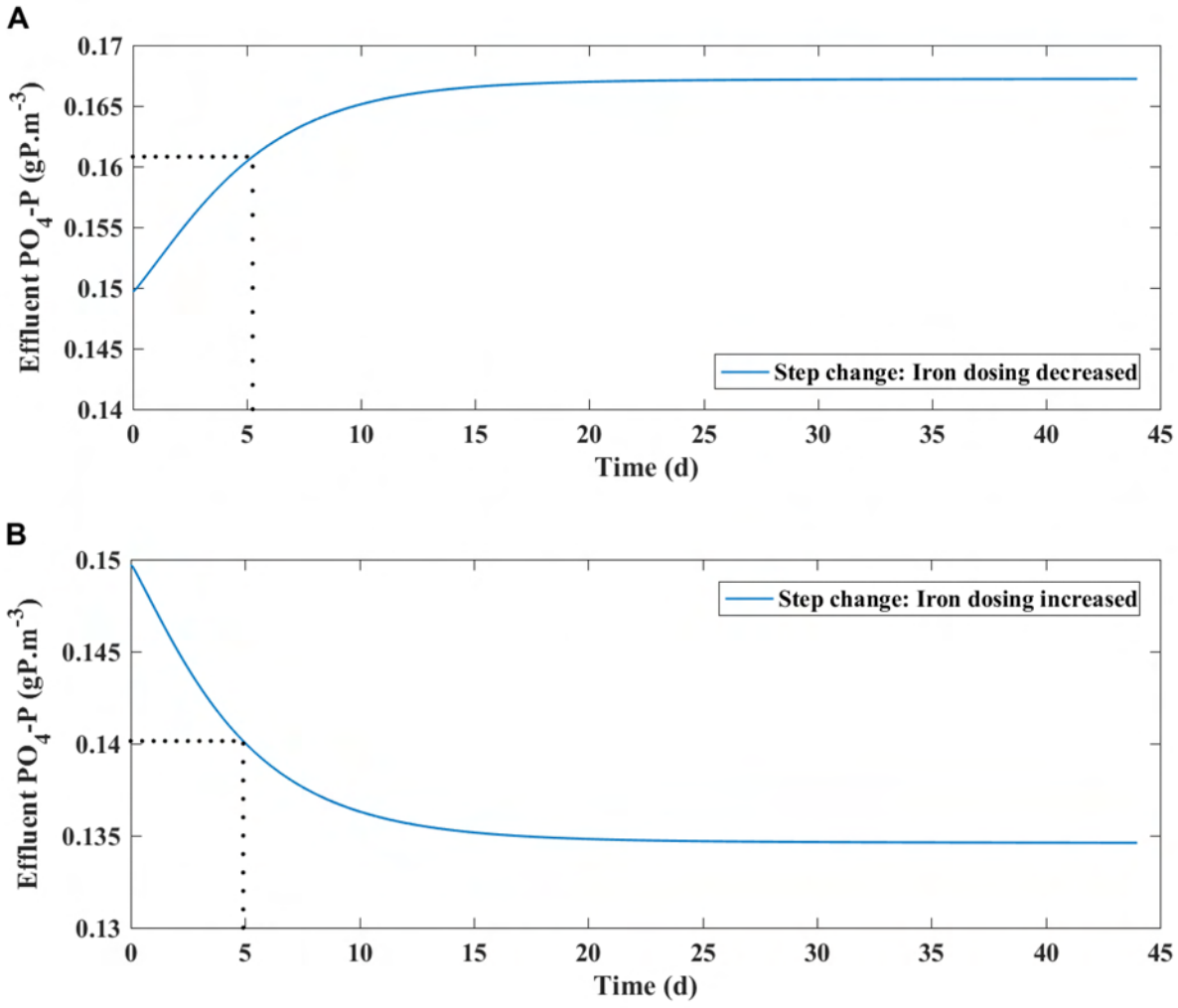
A
Effluent PO4-P (gP.m-3)
0.17
0.165
0.16
0.155
0.15
0.145
0.14
0
5
10
15
20
25
30
35
40
45
Time (d)
Step change: Iron dosing decreased
B
Effluent PO4-P (gP.m-3)
0.15
0.145
0.14
0.135
0.13
0
5
10
15
20
25
30
35
40
45
Time (d)
Step change: Iron dosing increased

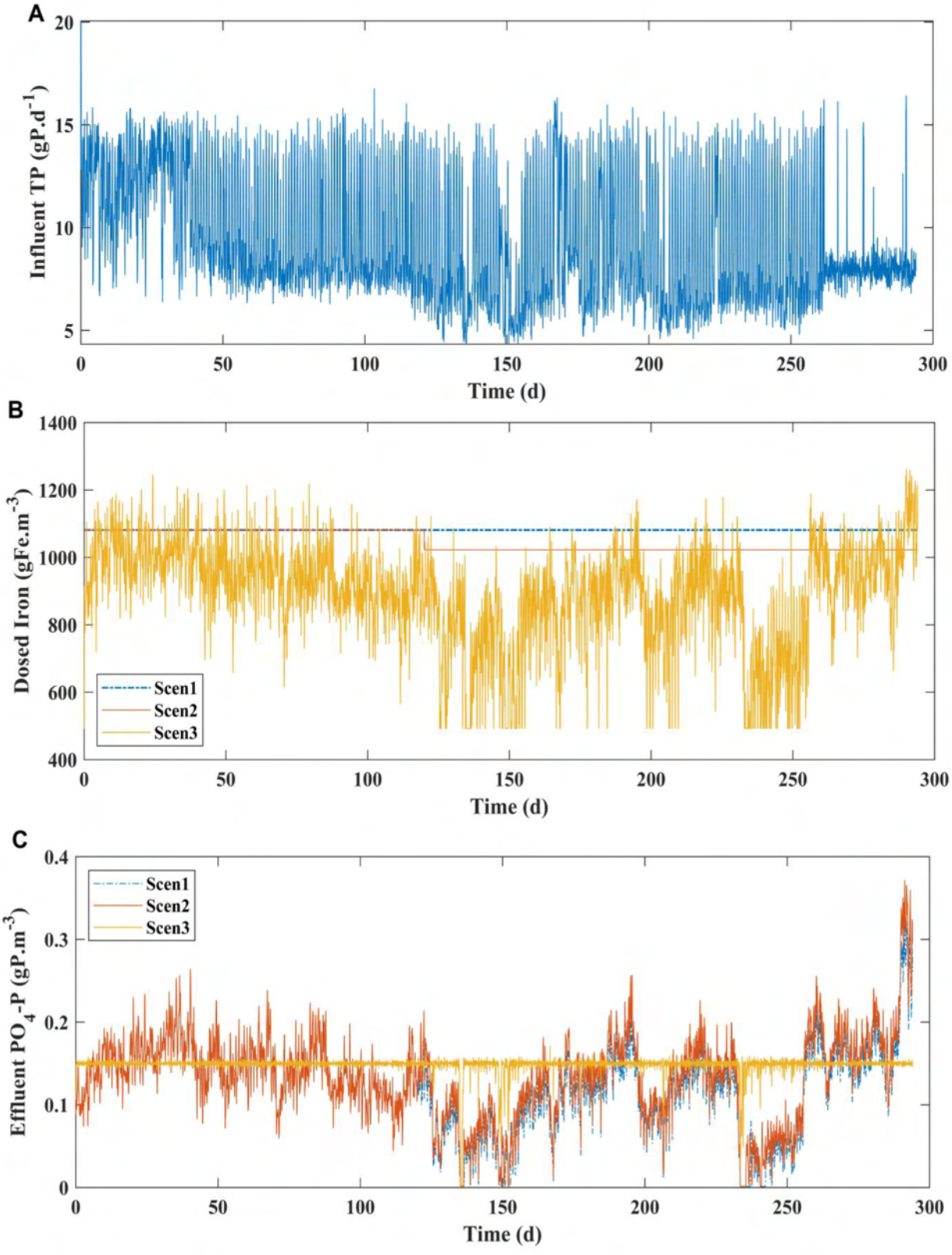
A
Influent TP (gP.d-1)
Time (d)
B
Dosed Iron (gFe.m-3)
Scen1
Scen2
Scen3
Time (d)
C
Effluent PO4-P (gP.m-3)
Scen1
Scen2
Scen3
Time (d)

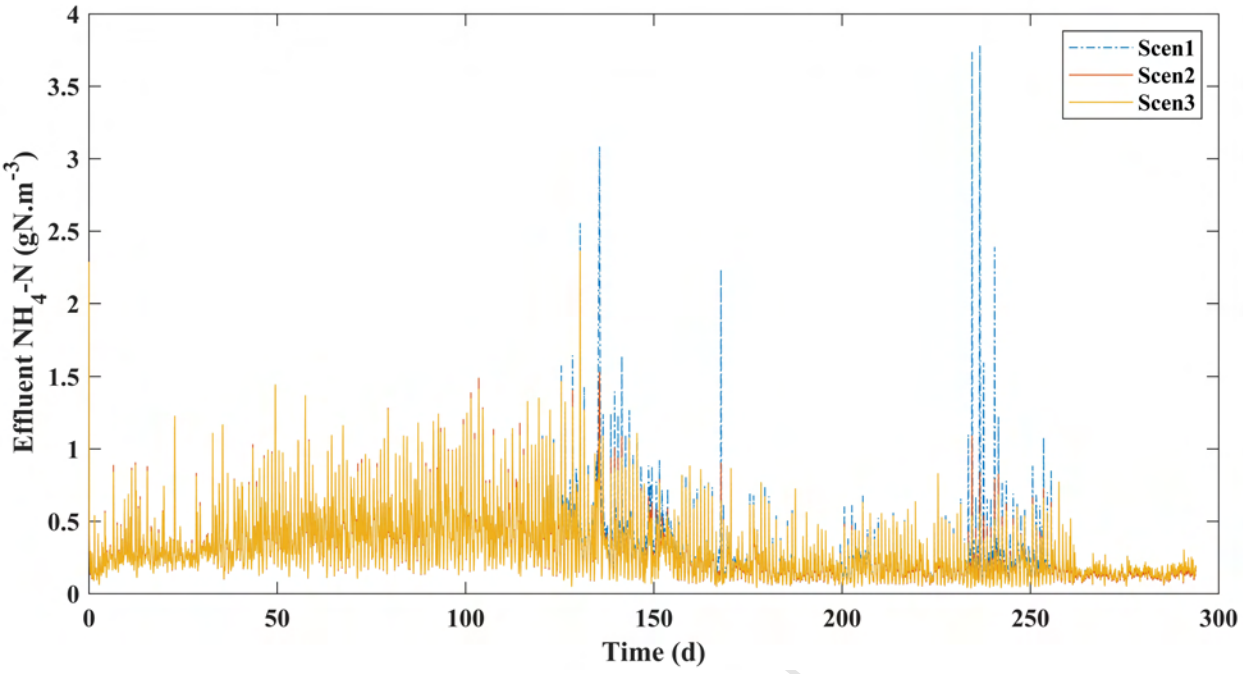

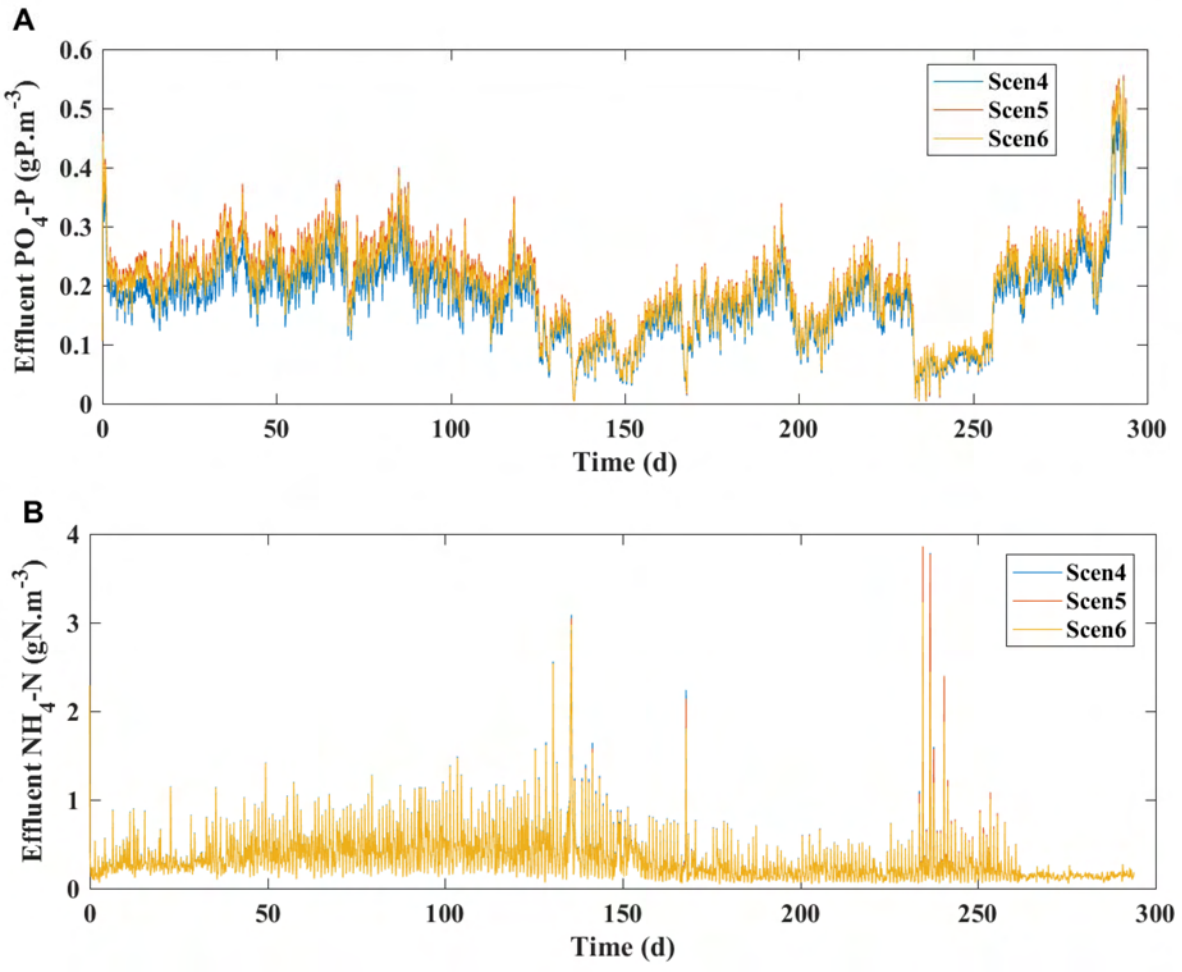
A
Effluent PO4-P (gP.m-3)
Time (d)
Scen4
Scen5
Scen6
B
Effluent NH4-N (gN.m-3)
Time (d)
Scen4
Scen5
Scen6

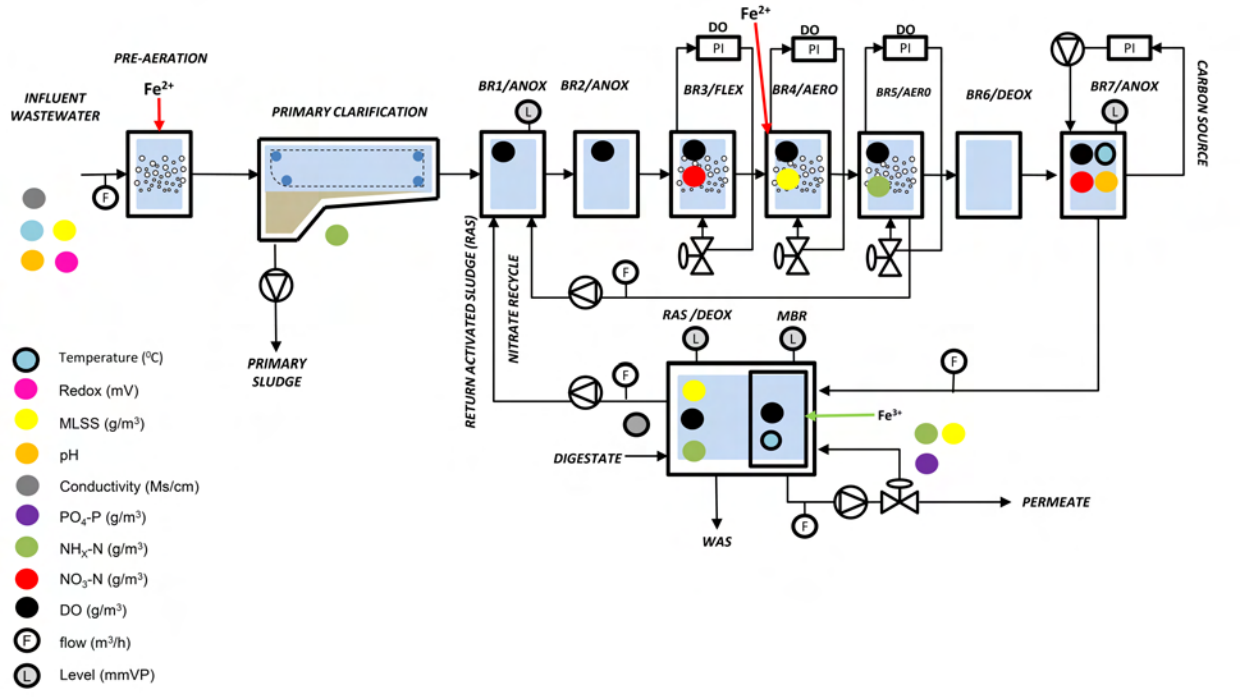

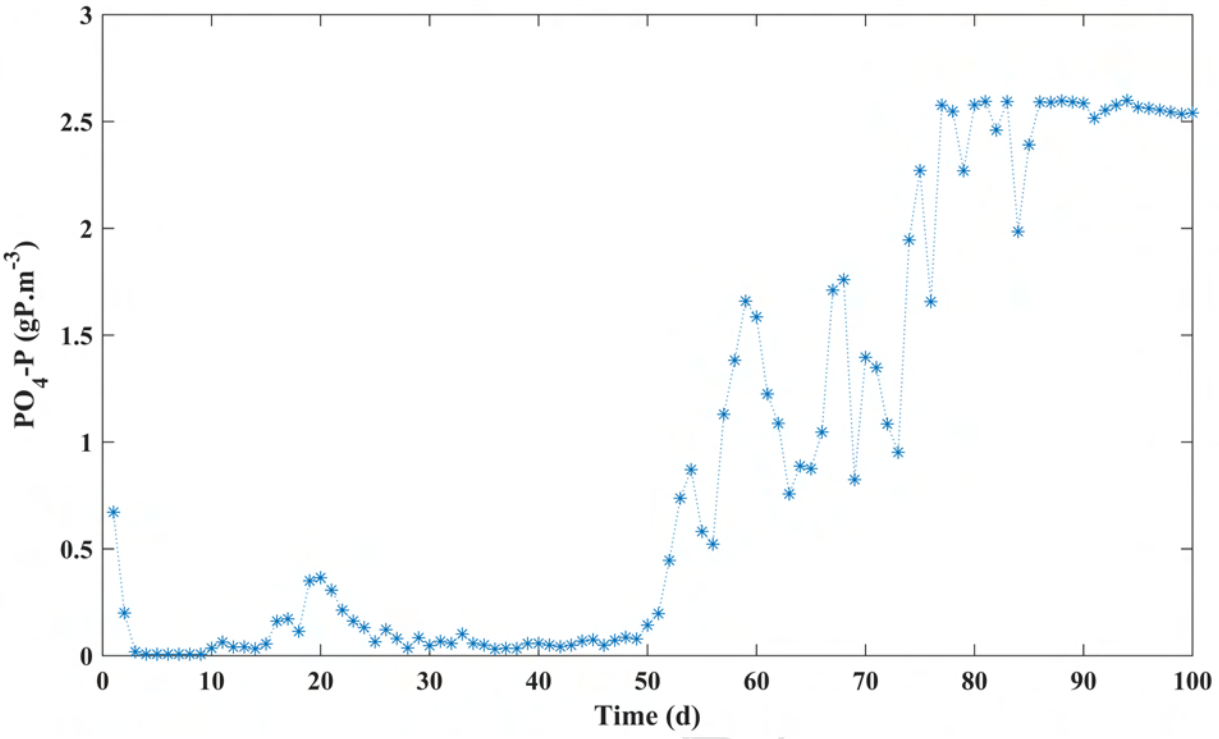

Research Highlights

- A plant-wide model calibrated against extensive pilot-plant data describing phosphorus (P) dynamics with iron (Fe) dosing
- Good agreement between measured and modelled P (5–10% (relative) difference).
- P concentration strongly depends on pH, Fe/P ratio and influent P load.
- P removal control strategies substantially reduce $FeSO_4$ dose.
- Model shows aerobic tanks are the most suitable dosing location for $FeSO_4$, due to fast oxidation of Fe^{2+} to Fe^{3+}.